Laminar Flow Heat Transfer Enhancement in Square and Rectangular Channels having: (1) a Wire-Coil, Axial and Spiral Corrugation Combined with Helical Screw-Tape with and without Oblique Teeth and a (2) Spiral Corrugation Combined with Twisted Tapes with Oblique Teeth

[*]**Madhu Sruthi Emani**[a]
e-mail: **sruthi.emani@gmail.com**

[*]**Hrishiraj Ranjan**[a]
e-mail: hrishi.ssec@gmail.com

[*]**Anand Kumar Bharti**[a]
e-mail: anandkumar.kumar908@gmail.com

[1]**Prof Josua P Meyer**[b]
e-mail: josua.meyer@up.ac.za

[*]**Sujoy Kumar Saha**[a]
e-mail: **sjykmrsh@gmail.com**

[a]Mechanical Engineering Department, Indian Institute of Engineering Science and Technology Shibpur, Howrah 711103, West Bengal, India
[b]Department of Mechanical and Aeronautical Engineering, University of Pretoria, Private Bag X20, Hatfield 0028, South Africa

[1]Corresponding Author

HIGHLIGHTS

- Laminar flow through non-circular ducts with inserts is studied experimentally.
- Uniform wall heat flux boundary condition is imposed on the channel outer wall.
- Wide Prandtl number range is covered using viscous Servotherm medium oil.
- Heat transfer and pressure drop characteristics against Reynolds number are plotted.
- Correlations developed and performance evaluation is done and these are beneficial.

ABSTRACT

Heat transfer enhancement is a vital area of research as it helps to design heat exchangers of reduced sizes and improved heat transfer rates. Thus, there is a pressing need for techniques which result in significantly increased heat transfer over and above increased pressure drop. In this paper, the benefits of different compound techniques using (1) wire-coil inserts and helical screw-tape inserts with oblique teeth, (2) wire-coil inserts and helical screw-tape inserts without oblique teeth, (3) spiral corrugation and helical screw-tape inserts without oblique teeth, (4) axial corrugation and helical screw-tape inserts without oblique teeth, (5) spiral corrugation and twisted-tape inserts with oblique teeth were studied experimentally for laminar flow in a non-circular duct (aspect ratio = 1, 0.5 and 0.33). Servotherm medium oil with Prandtl number ranging from 430 to 530 was used as working fluid. The experiment was conducted for a uniform heat flux boundary condition. The effect of geometric parameters of the inserts such as wire-coil diameter, wire-coil helix angle, tooth angle and tooth horizontal length of the screw tape and the twisted tape, corrugation height and corrugation pitch, etc. on heat transfer and pressure drop characteristics was presented. The influence of duct geometry (aspect ratio) on Nusselt number and friction factor was also studied. Correlations for Nusselt number and friction factor were developed and a performance evaluation was done.

Keywords: *Laminar flow, convection, coil, screw tape, swirl*

1. INTRODUCTION

Heat transfer augmentation is a subject of immense importance in increasing the heat transfer rate and achieving higher energy efficiency in thermal management. The heat transfer augmentation techniques are classified into passive, active and compound methods [1]. The study of different passive inserts has proved to be an effective heat transfer enhancement technique for heat exchangers. Insert devices are primarily used for single-phase flow and these enhancement techniques increase the tube-side convective heat transfer. Insert devices involve various geometric forms and these are inserted into smooth tubes. Performance and initial cost dictate which method will be preferred.

The use of various enhancement techniques to augment the convective heat transfer coefficient inside tubes has been investigated for many years. Insert devices are best suited to laminar flow. For turbulent flow, insert devices are not good. Nevertheless, insert devices are quite suitable for making the performance of an existing heat exchanger better. The high cost of energy and material has resulted in increased research into production of more efficient heat exchange equipment [2]. Though several designs for inserts have been proposed, most of them are too complex to be manufactured and they also lead to high pressure drops. The use of simple wire-coil inserts, twisted-tape inserts, screw-tape inserts, etc. in laminar flow through channels has resulted in better performance in comparison with that of smooth channels. The interesting features of the inserts and their promising potential in many heat transfer applications such as heat exchangers, nuclear reactors, solar heaters, gas turbines and combustion chambers have prompted different studies [3]. Some of the important works in literature are presented here.

Twisted-tape inserts make the flow helical, imparting swirl into the flow with the addition of radial velocity and tangential velocity to the main axial velocity along the axis of the channel. The more the swirl intensity is, due to tighter twist in the tape, the more the enhancement is. However, the tape inserts seldom have good thermal contact with the tube wall and the twisted tapes do not act as a fin.

Abolarin *et al*. [4] studied the effect of alternating clockwise and counterclockwise twisted-tape (CCCTT) inserts on heat transfer and pressure drop characteristics in transitional flow. Safikhani and Abbasi [5] worked on heat transfer

enhancement by using twisted-tape inserts with some modified twisted-tape inserts. Qi *et al*. [6] studied the effect of twisted-tape structures on thermohydraulic performances of nanofluids in a triangular tube. Liu *et al*. [7] proposed a new type of coaxial cross-twisted tapes for high viscous oil to enhance the heat transfer rate in laminar flow.

Extended surface inserts are the extruded shapes inserted into the tube; the tube is drawn to provide good thermal contact between the wall and the insert. The insert reduces the hydraulic diameter and acts as an extended surface. The extended surface insert is suitable for both laminar flow and turbulent flow, but it is costly. Mesh or brush inserts are displaced insert devices and these devices are displaced from the tube wall and they cause periodic mixing. Displaced enhancement devices are better suited to laminar flow than to turbulent flow, since the thermal impedance is not confined to a thin boundary layer region near the wall in laminar flow, according to Oliver and Aldington [8]. Abu-Mulaweh [9] carried out an experimental study to compare four different types of heat transfer enhancement techniques: two insert devices (displacement device and swirl flow device), extended surfaces and obstruction devices.

For turbulent flow, the dominant thermal resistance is very close to the wall and it is, therefore, more effective to mix the flow in the viscous boundary layer at the wall than it is to mix the gross flow. Integral internal roughness provides enhancement with a higher efficiency index than provided by a wire-coil insert. In the laminar flow regime, the dominant thermal resistance is not limited to the thin boundary layer adjacent to the flow. Enhancement devices mixing the gross flow are more effective in laminar flow than in turbulent flow. The twisted-tape and mesh inserts are more suited to laminar flow. But because the tape is not in good thermal contact with the wall, its swirl-generating ability cannot be fully exploited.

The wire-coil insert is a type of roughness which is wall-attached and its behaviour is more akin to that of special helical ribs, Chen and Zhang [10] and Sethumadhavan and Raja Rao [11]. Herring and Heister [12] carried out an experiment to improve the performance of a compact heat exchanger by using wire-coil inserts in a tube. Khatua *et al*. [13] studied the condensation phenomenon of refrigerant R245fa in a tube fitted with wire-coil inserts. Gunes *et al*. [14] experimentally studied the effect of triangular cross-sectioned wire-coil inserts on heat transfer and pressure drop

characteristics. Sarac and Bali [15] examined the swirl flow in a horizontal tube which was generated by vortex generator with propeller-type geometry. Eiamsa-Ard *et al*. [16] used propeller-type swirl generator with varying pitch ratios and studied their heat transfer and pressure drop characteristics. Sundar and Sharma [17] carried out an experimental investigation on friction factor and heat transfer characteristics in a circular tube using longitudinal strip inserts.

Integral internal fins and roughness require deformation of the material on the inside surface of a long tube. The deformation of the inner surface of a tube must be manufactured in a cost-effective manner. Uttarwar and Raja Rao [18] experimentally studied the performance of various types of inserts such as rib roughness, wavy strip, twisted-tape and wire-coil and for all of them, they observed, in general, beneficial effects of the enhancement devices for the design of compact heat exchangers. Tiwari and Saha [19] observed the useful effect of combined use of transverse ribs and twisted tapes in laminar flow. Laminar and transitional flow heat transfer enhancement by wire insert has been done by Garcia *et al*. [20]. Agostini *et al*. [21] extensively reviewed state-of-the-art high heat flux cooling technologies using enhancement techniques. Helical screw-tape inserts were used as enhancement technique and an experimental study was made by Sivashanmugam and Suresh [22]. Jaisankar *et al*. [23] experimentally studied hydrothermal characteristics for twisted-tape-generated swirl flow.

Saha and co-authors presented intensive data on the performance of a combination of passive inserts for heat transfer enhancement in flow through circular, square and rectangular channels. Rout and Saha [24] studied heat transfer and pressure drop characteristics in flow through a pipe using compound technique which consisted of wire-coil and helical screw-tape inserts. Saha [25] presented the performance of compound technique for laminar flow through a pipe with integral helical corrugations fitted with a helical screw-tape insert. Saha [26] studied the combined effect of transverse ribs and wire-coil inserts in rectangular and square ducts.

Pal and Saha [27] presented correlations for predicting Nusselt number and friction factor for laminar flow through square and rectangular cross-sectional channels. They used transverse ribs and twisted tapes with and without oblique teeth for achieving heat transfer enhancement. Saha [28] also studied the effect of using transverse ribs and

twisted-tape insert combination on heat transfer augmentation in turbulent flow through non-circular channels.

Saha et al. [29] presented the performance of a twisted tape with centre clearance inserted into a circular channel along with a wire-coil insert. They presented the heat transfer and pressure drop characteristics for laminar flow through a circular channel.

Pramanik and Saha [30] experimentally studied the performance of a combination of transverse rib turbulators and twisted-tape insert (full length, short length and regularly spaced) for heat transfer augmentation. They concluded that the combination of transverse ribs and full-length twisted tape resulted in better performance as compared with other combinations of inserts. The thermohydraulic performance of laminar flow through a circular channel with longitudinal strip inserts was presented by Saha and Langille [31]. They considered full-length, short-length and regularly spaced strips having different cross-sections (square, crossed and rectangular). The correlations for Nusselt number and friction factor were also presented. The compound technique of heat transfer augmentation using axial corrugation and twisted tape with and without oblique teeth was experimentally studied by Saha [32]. He presented the effect of different insert geometrical parameters on heat transfer and pressure drop characteristics. Oztop [33] studied effective parameters on second law analysis for semi-circular ducts in laminar flow and constant wall heat flux. Dagtekin et al. [34] analysed entropy generation through a circular duct with different shaped longitudinal fins for laminar flow.

In this paper, the results of an experimental investigation with the compound techniques consisting of (1) wire-coil insert and helical screw-tape insert with oblique teeth, (2) wire-coil insert and helical screw-tape insert without oblique teeth, (3) spiral corrugation and helical screw-tape insert without oblique teeth, (4) axial corrugation and helical screw-tape insert without oblique teeth, (5) spiral corrugation and twisted-tape insert with oblique teeth were used to study the heat transfer and pressure drop characteristics of laminar fluid flow. All these are the innovative fin geometry combinations which have never been investigated before; encouraging and industrially useful results have been obtained which are likely to give more cost-effective heat exchangers. The details of the geometry of the wire-coil insert, spiral corrugation and

axial corrugation are shown in Figure 1. The helical screw-tape insert and twisted-tape insert with oblique teeth geometry are shown in Figure 2.

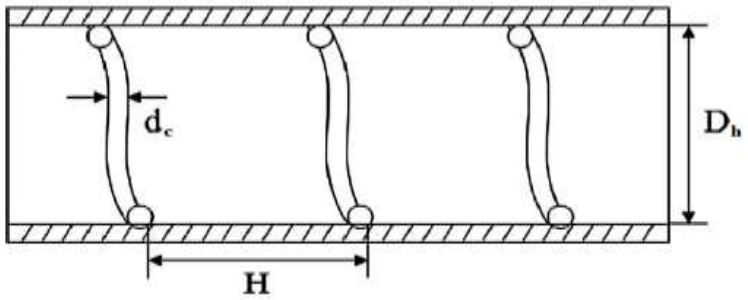

(a)

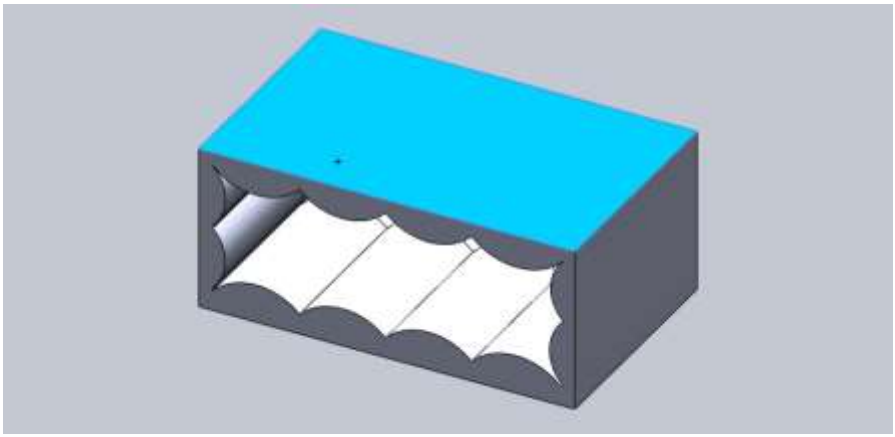

(b)

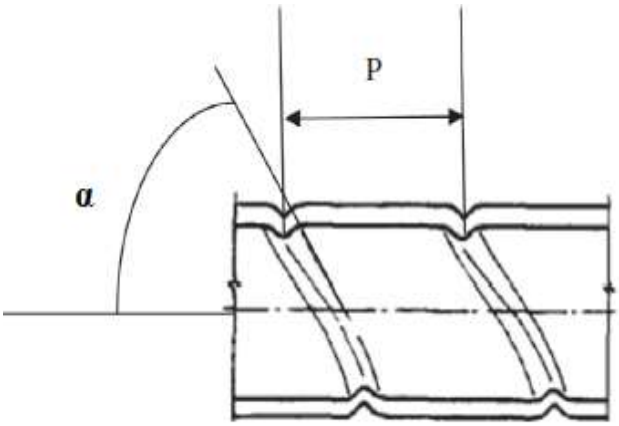

(c)

Fig. 1: Geometry of (a) wire-coil insert, (b) axial corrugation and (c) spiral corrugation geometry

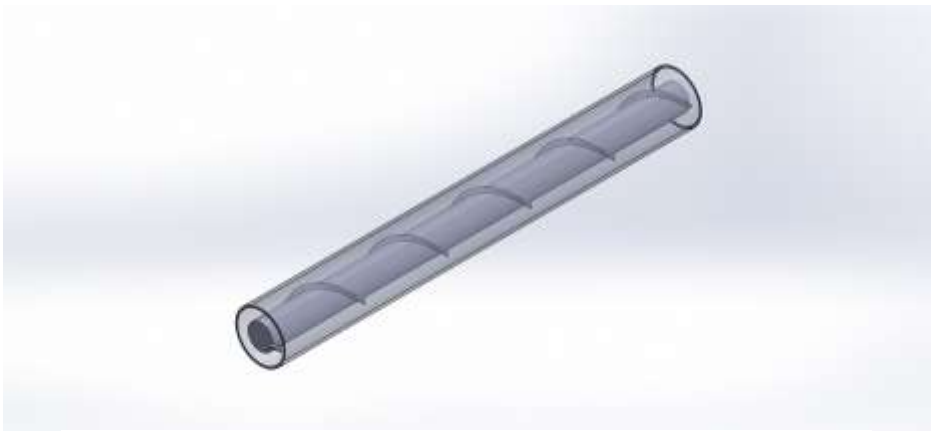

(a)

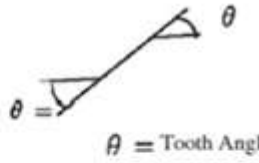

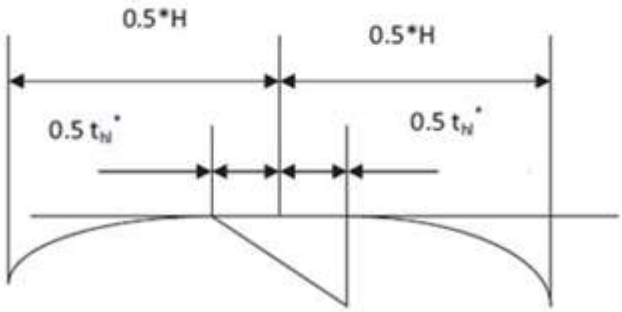

(b)

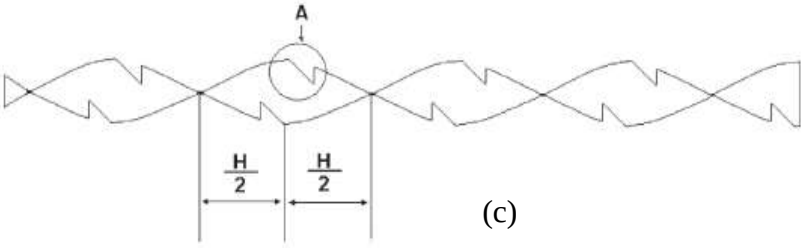

(c)

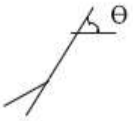

Θ=Tooth Angle

Fig. 2: Geometry of (a) screw-tape insert with oblique teeth, (b) oblique teeth and (c) full-length twisted-tape insert with oblique teeth

2. EXPERIMENTAL SET-UP, EXPERIMENTAL PROCEDURE AND DATA ANALYSIS

The hydrothermal transport tests were carried out in 2.0 m long brass channels having aspect ratio 1.0, 0.5 and 0.33. The friction, momentum, pressure and drag loss tests were carried out in an acrylic channel. Figure 3 shows the schematics of the test rig. The inserts were made of brass. Servotherm medium oil with Prandtl number range (430-530) was the working fluid. The working fluid was stored in a PVC tank (90 cm x 39.5 cm x 50 cm). A 2 kW Vane-type pump was used to circulate the oil to the test section through an accumulator whose function was to reduce pressure fluctuations and oil hammering. The excess oil was returned to the oil reservoir tank by means of an oil bypass pipe. Three rotameters (0.07—0.7, 0.0115—0.115 and 0.00175—0.0175 kg/sec) were used for measuring and regulating the oil mass flow rate to the test section. A calming section (25 mm diameter and 1.2 m length), made of GI pipe, ensured that the flow was hydrodynamically developed before the fluid entered the test section. The mean temperature of the fluid at the test section outlet was obtained by allowing the fluid to pass through a mixing chamber, which was followed by an oil cooler, where the working fluid was cooled and sent back to the oil storage tank to get recycled.

Copper-constantan thermocouple wires of 34 gauge were embedded on the tube outer surface at seven axial stations (i.e. at 0.05, 0.5,1.0, 1.25, 1.5, 1.75 and 1.95 m respectively from the test section fluid inlet) to measure the outer-wall temperature. At each axial station, four thermocouples were embedded circumferentially 90° apart. The measurement of fluid inlet and exit temperature was done with thermocouple wires embedded at the calming section and at the mixing chamber outlet respectively.

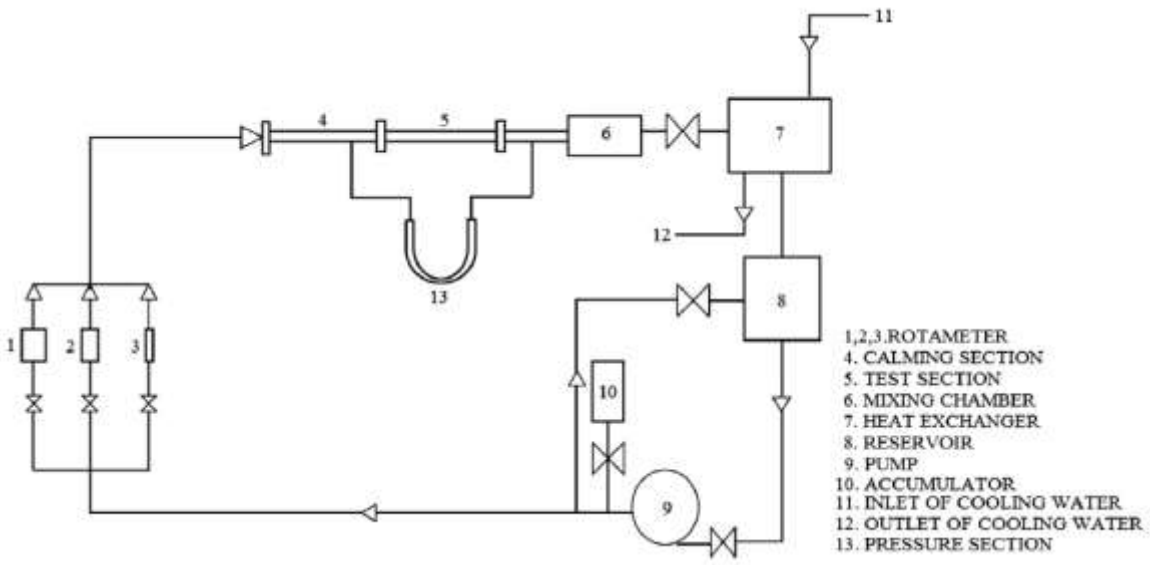

Fig. 3: Schematic representation of experimental rig

The magnitude of constant heat flux to the test section was varied by varying the voltage through autotransformers. To measure the electrical energy input, digital voltmeter and ammeter were connected in parallel and in series respectively to the autotransformers. A digital multimeter displayed the temperature in millivolt, from which using a conversion factor (40 μV=1 °C, obtained when the digital multimeter was calibrated between 100 °C and 0 °C), the equivalent outer-wall tube temperatures were recorded.

Pressure drop across the test section was measured using a U-tube mercury manometer. In the cooling water circulating loop, cool water was pumped from the ground water reservoir to the overhead tank using centrifugal pump and then water from the overhead PVC tank passed through the oil cooler under gravity, where it cooled the working fluid.

The set-up was allowed to run for an hour or more for particular mass flow rate and uniform heat flux input to attain steady state. For regulating the mass flow rate,

control valves were provided at the inlet of the rotameters. Once steady state was attained, the outer-wall surface temperatures, fluid inlet and exit temperatures were recorded using the digital multimeter, which displayed voltage in millivolt. After the inlet and exit temperatures were recorded, fluid local temperature at seven axial stations was obtained by carrying out linear interpolation. This approach was nearly perfect because the fluid bulk mean temperature increased linearly under uniform heat flux condition. Peripheral local temperatures in an axial station were arithmetically averaged to get axial local temperatures and Nusselt numbers. Average Nusselt numbers based on local Nusselt numbers were obtained by applying the trapezoidal rule. The actual heat received by the oil was its enthalpy rise.

A thermocouple bead was insulated from the electrically heated tube-wall surface with a very thin fibreglass tape. This tape was wrapped in such a way that no bare surface of the tube was visible, thereby preventing any possibility of electric shock. To control the thermal losses from the test section, asbestos rope and glass wool were used. To keep the insulation assembly intact, the test section was finally wrapped with jute tape. Each test tube end was welded with the flange. The flange was made of stainless steel material. To insulate the test tube electrically, fibreglass tape was wrapped over the tube throughout the full length of the test section. Thermocouple beads (34-gauge copper-constantan) were embedded over the test tube at 28 places at 5 cm, 50 cm, 100 cm, 125 cm, 150 cm, 175 cm, 195 cm distance from the upstream end of the flowing fluid and at each place, there were four thermocouples around the periphery with equal gap. Heater wire (nichrome wire of 20 gauge and 1.6 Ω/m) of 31.7 m length with a porcelain bead was wrapped over half the length of the tube equally spaced to generate uniform wall

heat flux over the tube and by the same way, the other half of the tube was wrapped with the same length of nichrome heater wire. After the asbestos cord was wound over the test tube, glass wool was wrapped all over the test tube to ensure the test tube outside wall was fully adiabatic. The glass wool thickness was 120 mm to resist radial directional heat loss.

Experimental uncertainty was estimated following [35]. The uncertainties in Re, Pr, f and Nu were $\pm$ 4.3 %, $\pm$ 5.87 %, $\pm$ 6.33 % and $\pm$ 7.45 % respectively. A more detailed discussion of this section is provided in [36-40].

The combined inserts geometry used in this investigation are given below in Table A

Case (1)
Insert configuration for combination of wire-coil insert and helical screw-tape insert with oblique teeth:
W = 8 mm,
c = 2.5 mm (for AR 1.0), 4 mm (for AR 0.5) and 5.5 mm (for AR 0.33).
d = 0, 1.5 mm and 2 mm giving
Q = Wc/d = ∞, 13.33 mm and 10 mm (for AR 1.0); ∞, 21.33 mm and 16 mm (for AR 0.5); and
∞, 29.33 mm and 22 mm (for AR 0.33)
q = Q/D_h = ∞, 1.0867 and 0.769 (for AR 1.0); ∞, 1.301 and 1.0 (for AR 0.5); and ∞, 1.54 and 1.1579 (for AR 0.33); Oblique tooth angle: θ = 30°, 45° and 60°
Tooth horizontal length: t_{hl}^* = 1 mm, 1.5 mm and 2 mm
Dimensionless tooth lengths (horizontal): $t_{hl} = t_{hl}^*/D_h$ = 0.0769, 0.1248 and 0.1538 (for AR 1.0); 0.0625, 0.0944 and 0.12 (for AR 0.5); 0.0526, 0.071 and 0.10526 (for AR 0.33)
Coil helix angles: δ = 30°, 45°, 60°; Wire diameter: d_c = 1 mm; Dimensionless diameter (coil wire): 11
$d_{star} = d_c/D_h$ = 0.07692, 0.0625 and 0.0526
Case (2)
Insert configuration for combination of wire-coil insert and helical screw-tape insert without oblique teeth:
Screw-tape insert: 2 m long, W = 8 mm (fixed); c = 11 mm, 8.5 mm, 16.0 mm; d = 0, 1.5 mm, 2 mm and 2.5 mm
Q = W × c/d = ∞, 5.33 mm, 4 mm and 3.2 mm
Screw-tape parameter: q = Q/D_h = ∞, 2.72, 2.04, 1.63 (for AR 1.0); ∞, 3.68, 2.76, 2.21 (for AR 0.5);
and ∞, 6.16, 4.62, 3.69 (for AR 0.33)
Wire-coil helix angle: δ = 30° and 60°; Wire-coil diameter: d_c/D_h = 0.07692 and 0.1026

Case (3)
Insert configuration for combination of axial corrugation and helical screw-tape insert
without oblique teeth:
Screw-tape insert: 2 m long; W = 8 mm (fixed); c = 11 mm, 8.5 mm, 16.0 mm; d = 0, 1.5 mm, 2 mm and 2.5 mm
Q = W × c/d = ∞, 5.33 mm, 4 mm and 3.2 mm
Screw-tape parameter: $q = Q/D_h$ = ∞, 2.72, 2.04, 1.63 (for AR 1.0); ∞, 3.68, 2.76, 2.21 (for AR 0.5);
and ∞, 6.16, 4.62, 3.69 (for AR 0.33)
Corrugation angle: α = 30° and 60°; Corrugation pitch: P/h_c = 2.0437 and 5.6481

Case (4)
Insert configuration for combination of spiral corrugation and helical screw-tape insert
with oblique teeth:
Screw-tape insert: 2 m long; W = 8 mm (fixed); c = 11 mm, 8.5 mm, 16.0 mm
d = 0, 1.5 mm, 2 mm and 2.5 mm; q = Wc/d = ∞, 5.33 mm, 4 mm and 3.2 mm
Screw-tape parameter: $Q = q/D_h$ = ∞, 2.72, 2.04, 1.63 (for AR 1.0); ∞, 3.68, 2.76, 2.21 (for AR 0.5) and ∞, 6.16, 4.62, 3.69 (for AR 0.33)
Corrugation angle: α = 30° and 60°; Corrugation pitch: P/h_c = 2.0437 and 5.6481

Case (5)
Insert configuration for combination of twisted tape insert with oblique teeth and spiral corrugation:
Twisted-tape insert: 2 m long; Twist ratio: y = 2.5
Tooth horizontal length: t_{hl} = 0.05263, 0.07895 and 0.1053
Twisted-tape tooth angle: θ = 30°, and 60°; Corrugation helix angle: α = 30° and 60°
Corrugation height: h_c = 0.05263, 0.07895 and 0.1053

2. RESULTS AND DISCUSSION

At the outset of this section, it is noted that the friction plot is against Reynolds number, whereas for the Nusselt number, the plot is against ReX and NuY and the definitions of X and Y are given in the Nomenclature section; the flow has always been laminar, which is confirmed by the hydrothermal behaviour of the flow and the rather predictable slope of the trend curve.

Generally, in laminar flow, along with thermal resistance in the boundary layer formed near the wall, there is thermal resistance in bulk flow also. Wire-coil inserts and corrugations are mainly used to perturb the thin boundary layer along the wall and reduce thermal resistance. On the other hand, the helical screw-tape and twisted-tape inserts

generate swirl flow and enhance the mixing of the bulk fluid to reduce thermal resistance. Thus, in this paper, the results of an experimental programme using five different compound techniques consisting of wire-coil insert, axial and spiral corrugations, twisted-tape with oblique teeth and screw tape with and without oblique teeth inserted in a square and rectangular channel are presented (the specifics of the fin geometry of the combined inserts are given). The hydrothermal behaviour, predictive correlations and performance analysis are also presented. The principal objective of the experimental investigations was to see the relative effect of the geometrical parameters of the inserts and the channel on the hydraulic and thermal characteristics, friction factor and Nusselt number. Figure 4 and Figure 5 demonstrate the outcome of the confirmatory tests with bare ducts, which confirm the validity and reliability of the current experimental set-up. Nu, f and Re are defined with respect to the hydraulic diameter of the channel.

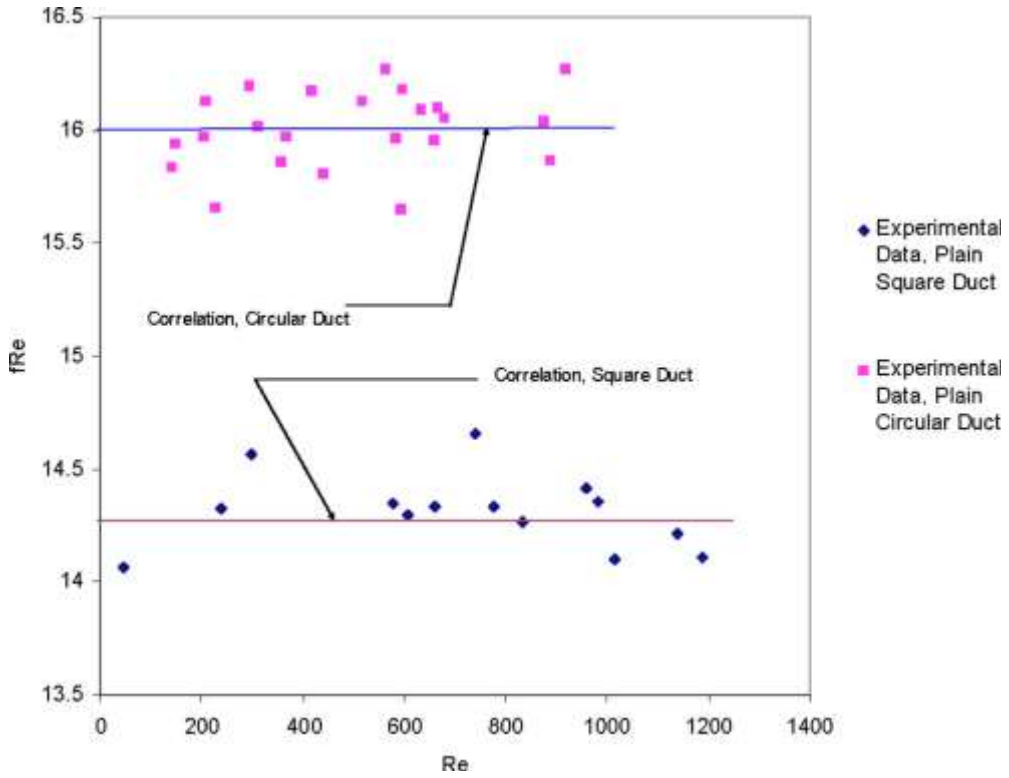

Fig. 4: Validation of experimental set-up for friction factor

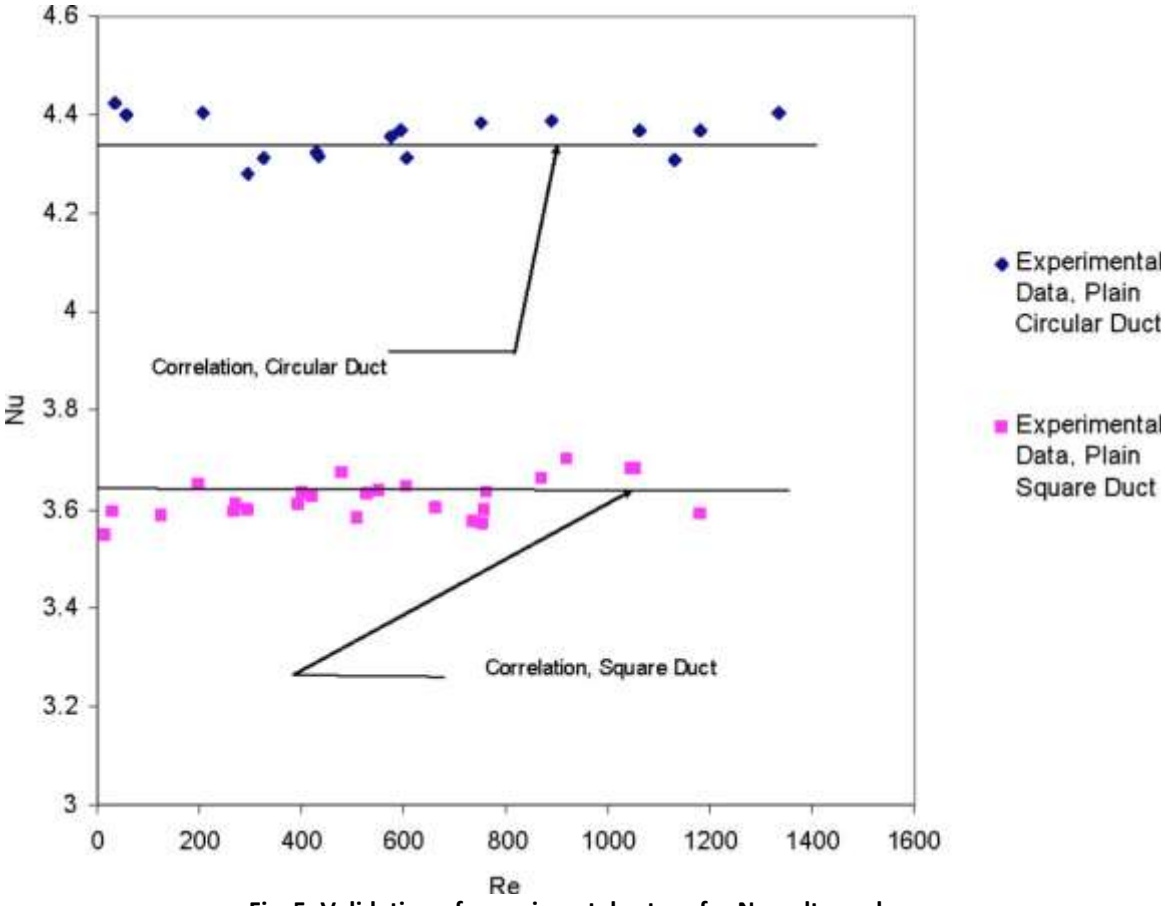

Fig. 5: Validation of experimental set-up for Nusselt number

Figure 6 and Figure 7 show the variation of friction factor and Nusselt number with Reynolds number respectively for different aspect ratios of the channel with wire-coil insert (WCI) and helical screw-tape inserts with oblique teeth (HSTOT). Also, these variations are compared with those obtained for a circular channel. The values of friction factor and Nusselt number for a circular channel are taken from Roy and Saha [3]. It is clear from Figure 6 that for a fixed tooth angle, helix angle and horizontal tooth length of the inserts, the friction factor increases with an increase in Reynolds number. This is due to the fact that, with an increase in Reynolds number, the velocity profile becomes much flatter, similar to the case of a turbulent flow. The friction factor for duct with aspect ratio = 0.33 is observed to be maximum while the minimum friction factor is noted for a

circular channel. This observation can be explained by the fact that the shallower cross-sectioned channel will have more secondary flow and recirculation, thereby causing added momentum loss and extra amount of pressure drop. It can also be observed that for duct flow, the friction factor values decrease with an increase in aspect ratio. Similarly, Figure 7 shows the variation of Nusselt number with Reynolds number for fixed geometry of the inserts. The Nusselt number values are found to be decreasing with increasing aspect ratio for the duct flow and maximum values are obtained for duct flow with aspect ratio = 0.33. Thus, as the aspect ratio decreases, the heat transfer rate and pressure drop both increase. This corroborates the trends of Reynolds analogy when the temperature profiles also behave in the same way as for the velocity profiles and also, the hydrodynamic boundary layer behaviour is in no way different from that of the thermal boundary layer. A similar trend can be observed in the case of other compound techniques employed in the experiment.

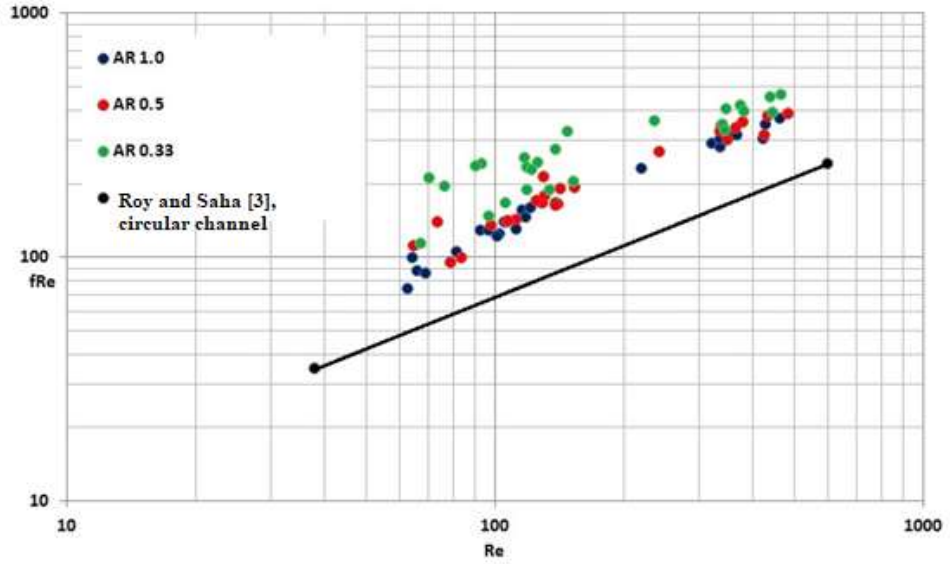

Fig. 6: Effect of aspect ratio on friction factor (q = 1.33, d_{star} = 0.0625, tooth angle = 45°, helix angle = 45°, horizontal tooth length = 0.1248) (WCI+HSTOT)

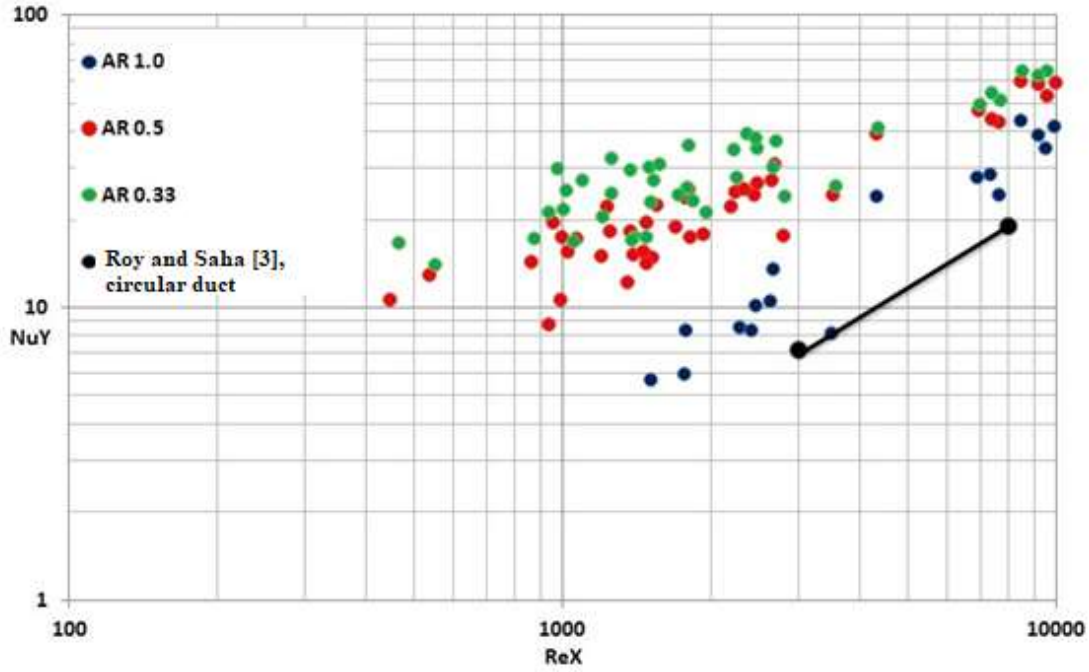

Fig. 7: Effect of aspect ratio on Nusselt number (q = 1.33, d_{star} = 0.0625, tooth angle = 45°, helix angle = 45°, horizontal tooth length = 0.1248) (WCI+HSTOT)

Figure 8 and Figure 9 show the effect of wire-coil diameter on heat transfer and pressure drop characteristics. The figures are shown for a combination of the WCI and HSTOT case. Friction factor and Nusselt number are plotted for different non-dimensional wire-coil diameters. The increase in friction factor and Nusselt number with Reynolds number can be observed from the above figures. The friction factor increase with wire-coil diameter is shown in Figure 8 for horizontal tooth length = 0.0625, tooth angle = 30°, helix angle = 30°, q= ∞, aspect ratio = 1.0. The increase in Nusselt number with wire-coil diameter is plotted in Figure 9 for horizontal tooth length = 0.0625, tooth angle = 30°, helix angle = 30°, q= ∞, aspect ratio = 1.0. The above observation is explained by the fact that, with the increase in wire-coil diameter, however small it may be, the flow cross-sectional area decreases and the local flow velocity increases, thereby

giving more momentum loss and more vigorous fluid mixing causing increased friction factor and Nusselt number.

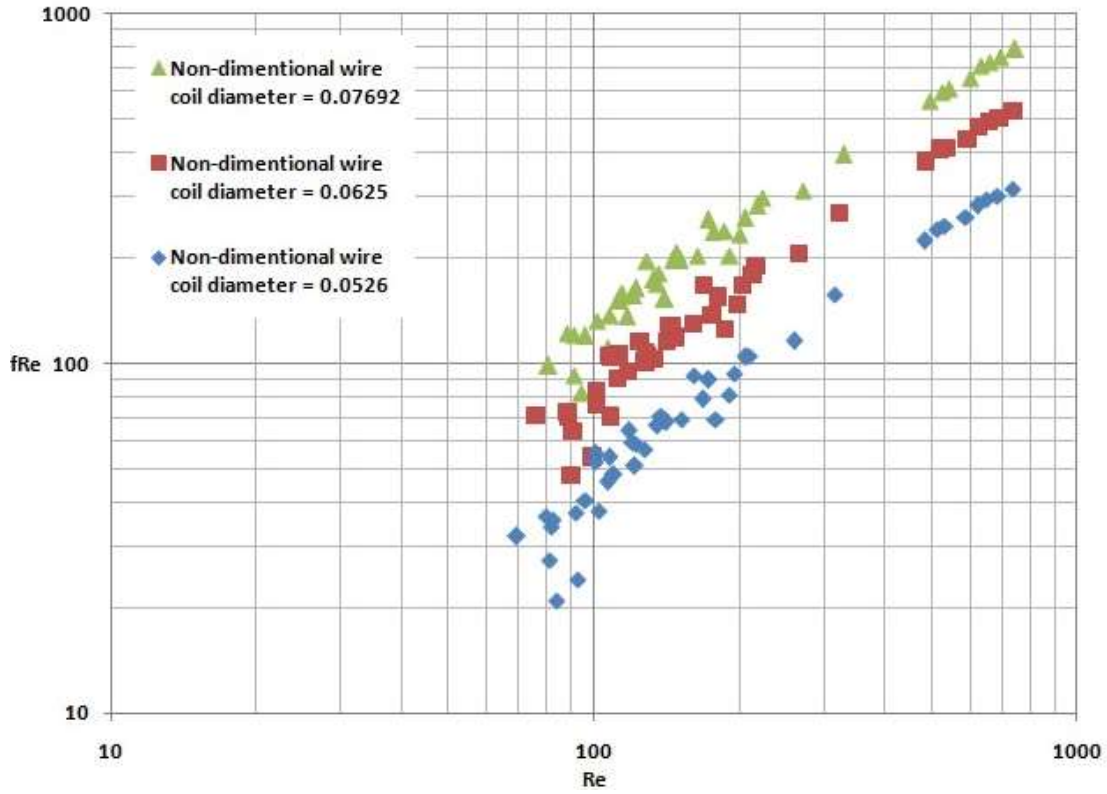

Fig. 8: Effect of wire-coil diameter on friction factor (horizontal tooth length = 0.0625, tooth angle = 30°, helix angle = 30°, q = ∞, aspect ratio = 1.0) (WCI+HSTOT)

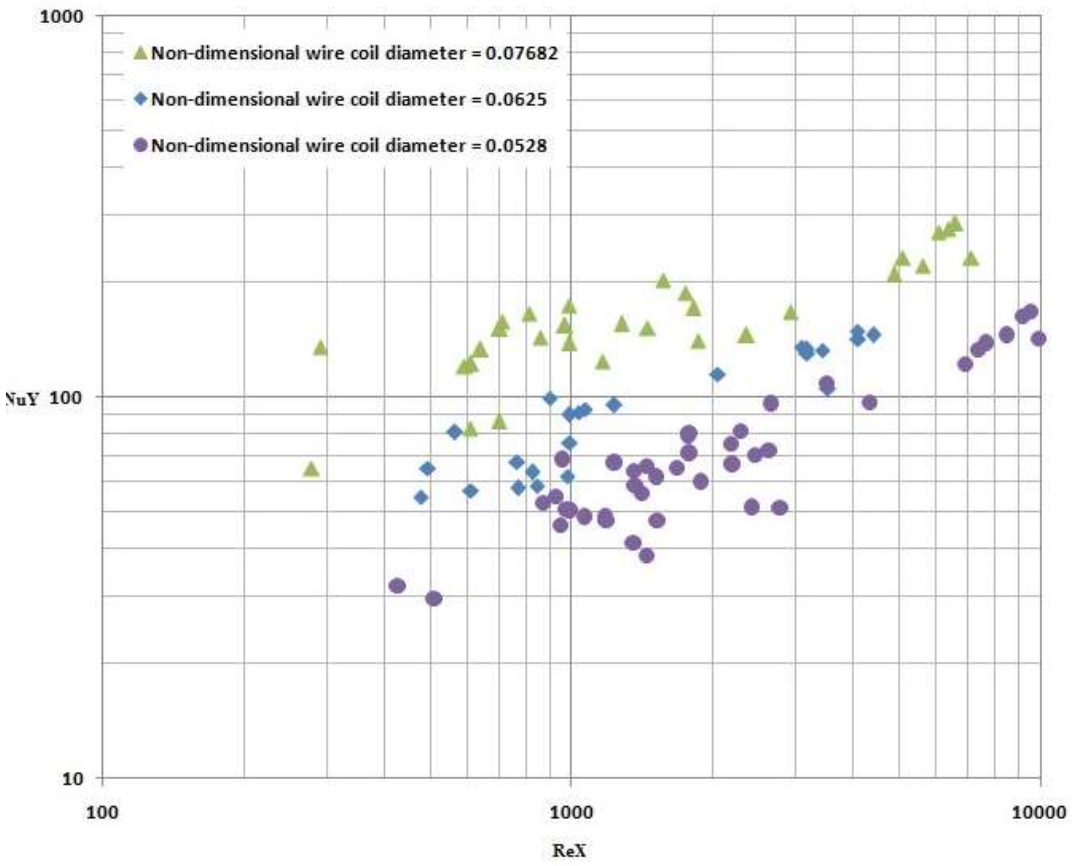

Fig. 9: Effect of wire-coil diameter on Nusselt number (horizontal tooth length = 0.0625, tooth angle = 30°, helix angle = 30°, q = ∞, aspect ratio = 1.0) (WCI+HSTOT)

Also, the effect of WCI helix angle is presented. An increase in friction factor with Reynolds number for coil wires having different helix angles can be seen in Figure 10. Three helix angles are considered for constant d_{star}= 0.0526, tooth angle = 45°, horizontal tooth length =0.0944, q= 1.301, aspect ratio = 1.0. The friction factor increases with an increase in the helix angle of the wire-coil insert. Thus, maximum friction and minimum friction are observed for 60° and 30° helix angles respectively. However, it can be noticed that no asymptotic rise or fall of friction factor and Nusselt number can be conjectured with the parametric values of the geometric dimensions. Figure 11 shows the variation of Nusselt number with Reynolds number for different helix angles of the wire-coil insert. The Nusselt number also increases with helix angle of the wire-coil insert.

The increase in Nusselt number with Reynolds number can also be observed in Figure 11. The variation of helix angle is done for constant values of d_{star}= 0.07692, tooth angle = 45°, horizontal tooth length =0.0944, q= 1.611, aspect ratio = 1.0. Similar to the friction factor case, the maximum and minimum Nusselt numbers are observed for helix angles 60° and 30° respectively. A similar effect of WCI diameter and helix angle is observed in the case of the second compound technique using WCI and helical screw-tape (HST) insert without oblique teeth studied here.

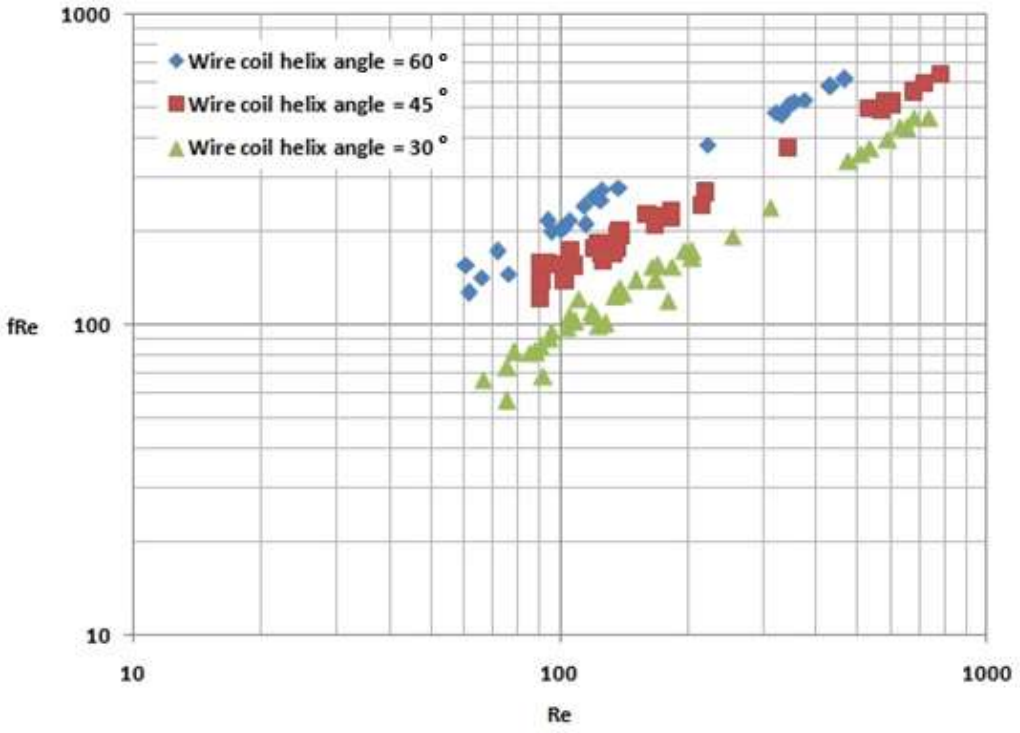

Fig. 10: Effect of wire-coil helix angle on friction factor (d_{star} = 0.0526, tooth angle = 45°, horizontal tooth length = 0.0944, q = 1.301, aspect ratio = 1.0) (WCI+HSTOT)

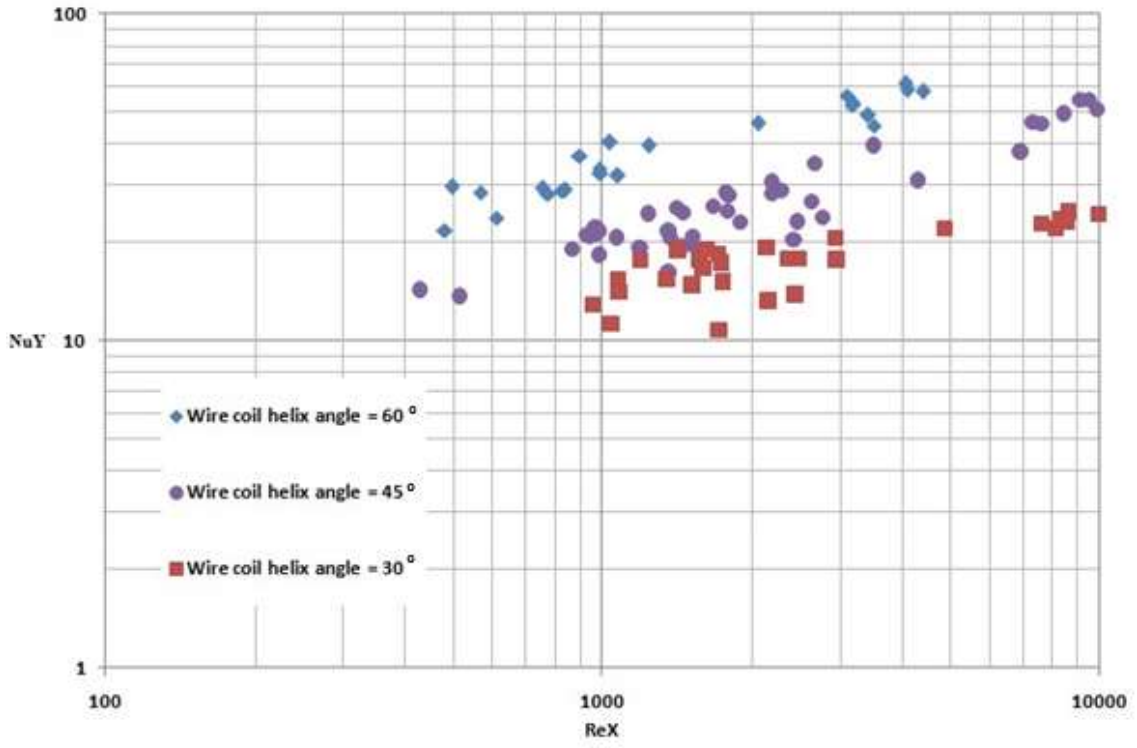

Fig. 11: Effect of wire-coil helix angle on Nusselt number (d_{star} = 0.07692, tooth angle = 45°, horizontal tooth length = 0.0944, q = 1.611, aspect ratio = 1.0) (WCI+HSTOT)

Nusselt number and friction factor are obtained for different cases in which three screw-tapes having oblique teeth angle 30º, 45º and 60º respectively are used along with wire coil of given geometry. The variation of friction factor with Reynolds number in the given laminar flow regime is shown in Figure 12. It can be observed that the friction factor increases with an increase in Reynolds number. It can also be clearly observed that the friction factor increases with an increase in tooth angle of the screw-tape inserts. Thus, the maximum friction factor is obtained with screw-tape having 60° tooth angle and the tape corresponding to 30° tooth angle shows the minimum pressure drop characteristics. Figure 13 presents a variation of Nusselt number with Reynolds number for screw-tape with different teeth angle and wire coil having a given geometry. The

Nusselt number is found to increase with the Reynolds number for all the inserts used. It is also observed that the screw-tape with 30º tooth angle and 60º tooth angle shows minimum and maximum values of Nusselt number respectively, whereas the screw-tape with 45º tooth angle shows the Nusselt number and friction factor values in between. The above observation is physically plausible because the larger tooth angle makes a deeper scar in the metal surface with more indenture on the flow and thereby causing both more profile and skin friction drag; and more intense fluid mixing gives a bigger Nusselt number.

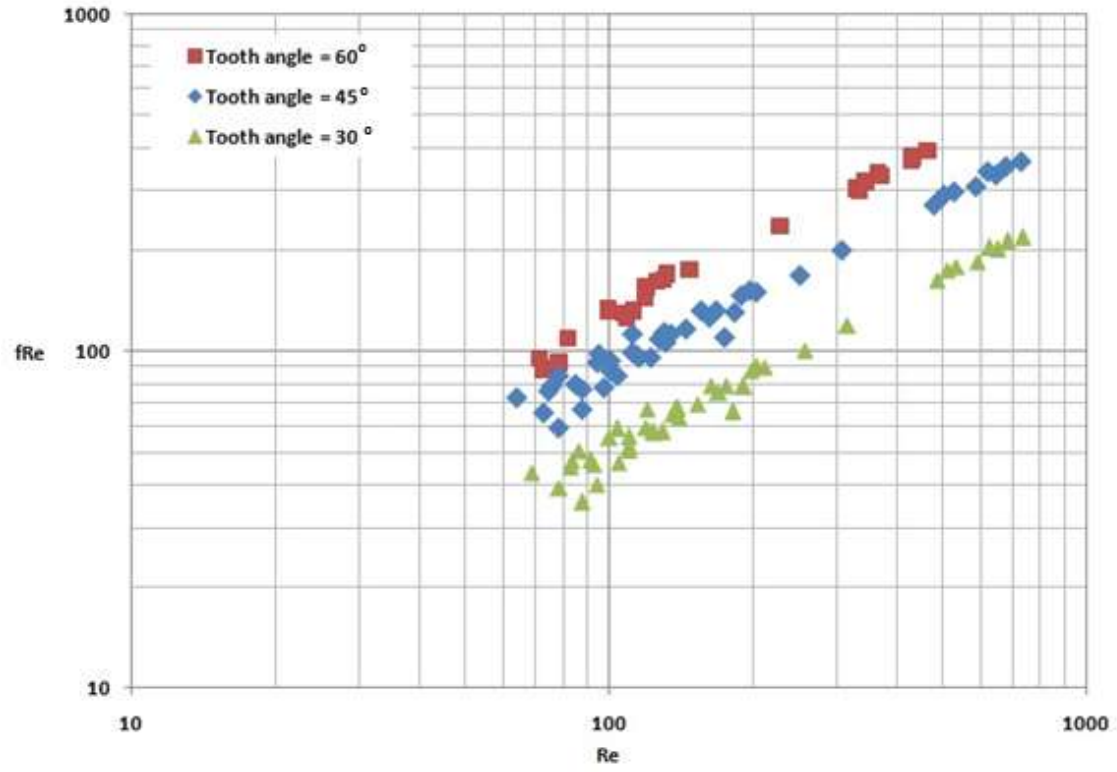

Fig. 12: Effect of tooth angle on friction factor (d_{star} = 0.07692, helix angle = 45°, horizontal tooth length = 0.0944, q = 1.611, AR = 1.0) (WCI+HSTOT)

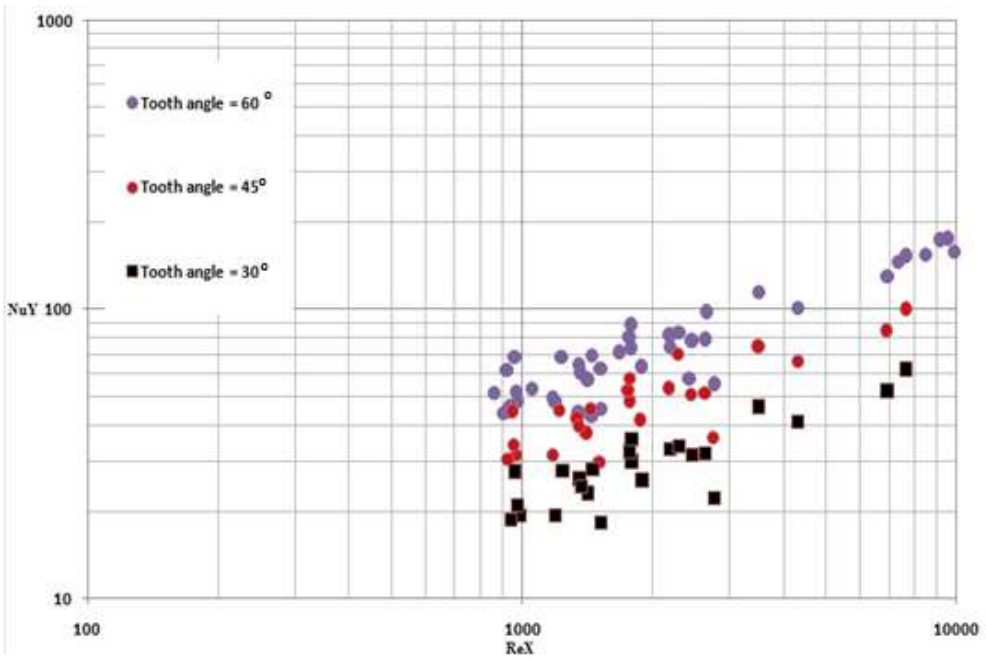

Fig. 13: Effect of tooth angle on Nusselt number (d_{star} = 0.07692, tooth angle = 45°, horizontal tooth length = 0.0944, q = 1.611, aspect ratio = 1.0) (WCI+HSTOT)

Figure 14 and Figure 15 show the impact of variation of tooth horizontal length on friction factor and Nusselt number. The tooth horizontal length is varied for d_{star}= 0.0625, oblique teeth angle = 45°, helix angle =60°, aspect ratio = 1.0. The friction factor is noted to increase with Reynolds number. The friction factor also increases with tooth horizontal length. A similar trend is observed for Nusselt number. Nu increases with both Reynolds number and tooth horizontal length. The minimum and maximum are recorded at horizontal tooth length of 0.0625 and 0.1538 respectively for both friction factor and Nusselt number. A similar behaviour with tooth horizontal length and tooth angle can be explained by a similar fluid flow dynamics and thermal mechanics. In case of compound technique with spiral corrugation (SC) and twisted-tape insert with oblique teeth (TTOT), a similar trend in variation of friction factor and Nusselt number with the geometry of the oblique teeth is observed. This is due to the fact that the combined insert geometries in

the two cases are similar in nature, even though one case is a displaced enhancement geometry, whereas the other case is of an integral roughness. It essentially makes one conclude that the enhancement principle in the two cases does not have a very critical difference; this is more true in the case of a small Reynolds number when the inertia force is not of large magnitude and the viscous force prevails.

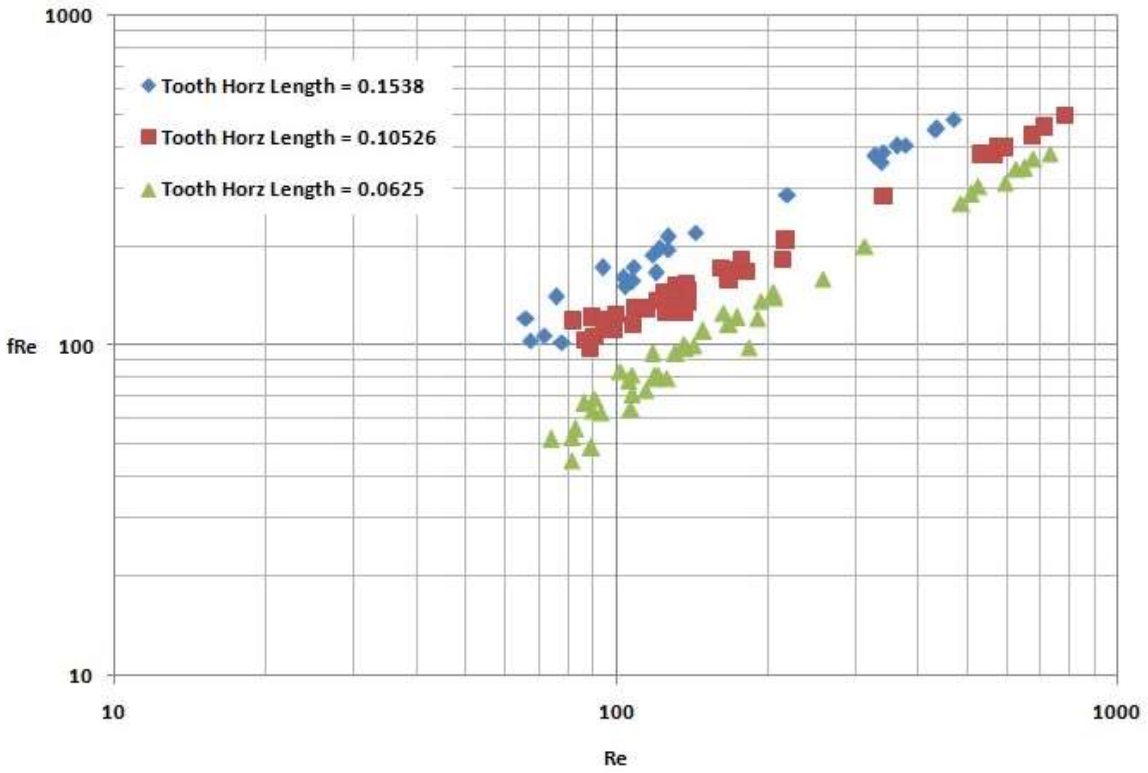

Fig. 14: Effect of tooth horizontal length on friction factor (d_{star} = 0.0625, oblique teeth angle = 45°, helix angle = 60°, q = 1.0867, aspect ratio = 1.0) (WCI+HSTOT)

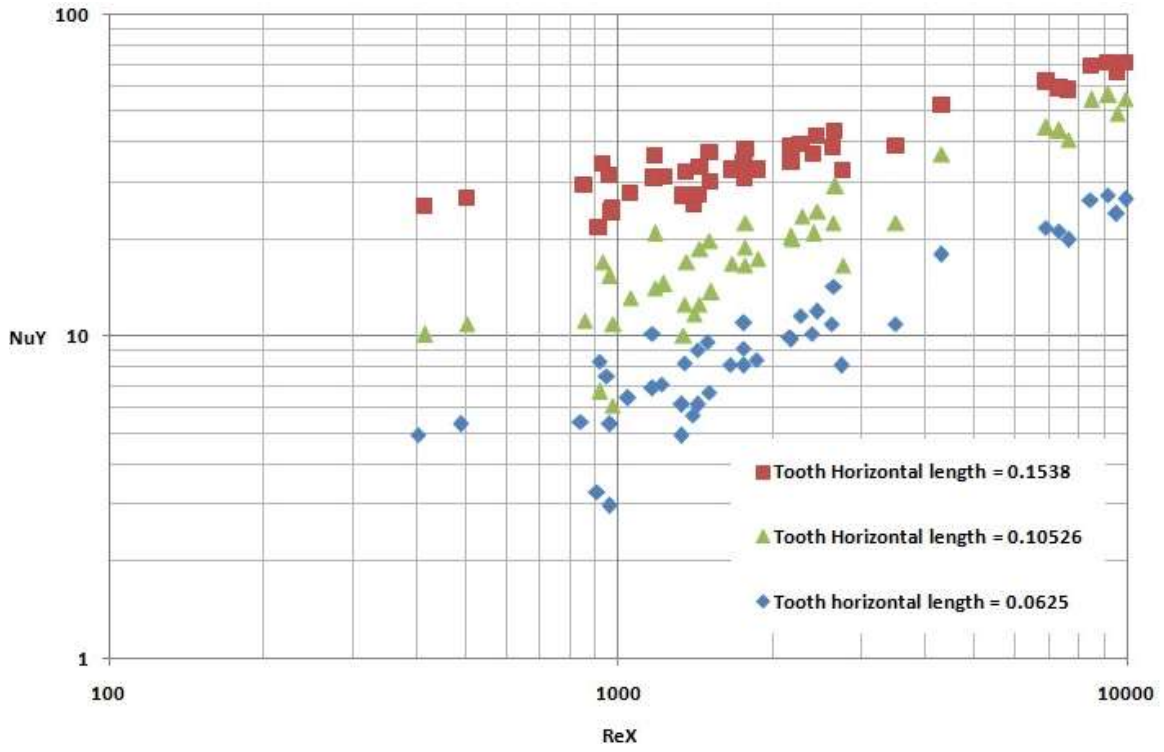

Fig. 15: Effect of tooth horizontal length on Nusselt number (d_{star} = 0.0625, tooth angle = 45°, helix angle = 60°, q = 1.0867, aspect ratio = 1.0) (WCI+HSTOT)

Figure 16 and Figure 17 show the effect of corrugation angle on friction factor and Nusselt number respectively. The effect of corrugation pitch and corrugation height is shown in Figures 18 to 21. It can be observed clearly that both friction factor and Nusselt number increase with angle and height of the corrugation, whereas the pitch effect is inverse. The thermohydraulic behaviour is well expected due to the very nature of the principle of enhancement.

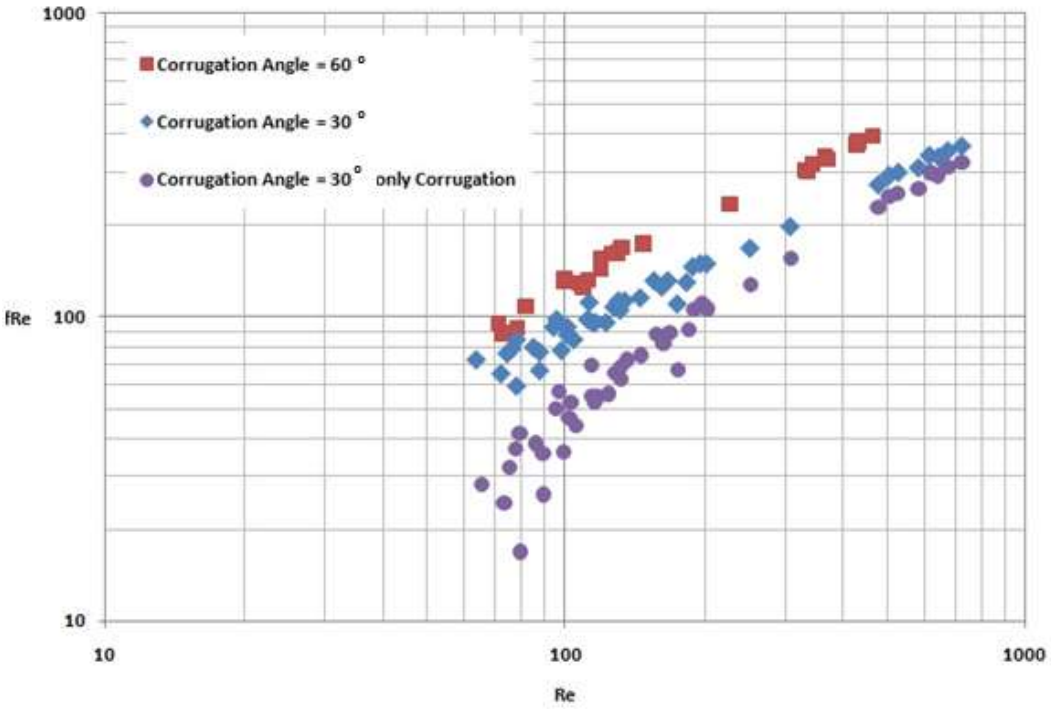

Fig. 16. Effect of corrugation angle on friction factor: q = 1.63, P/ h_c = 2.0437 (AC+HST)

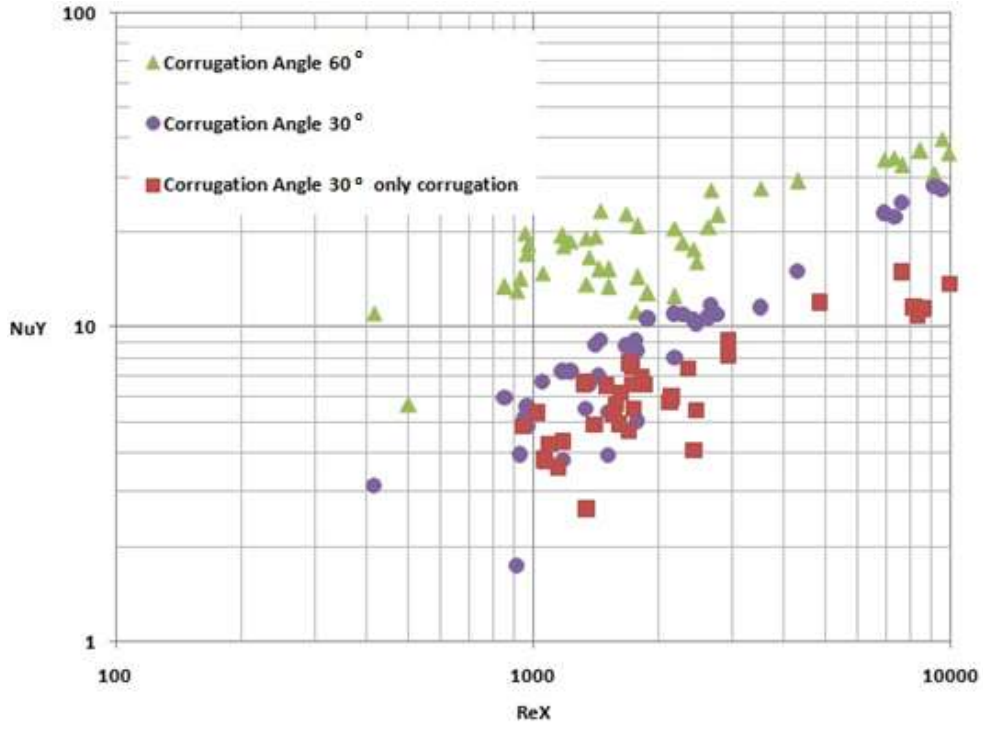

Fig. 17: Effect of corrugation angle on Nusselt number: q = 1.63, P/h_c = 2.0437 (AC+HST)

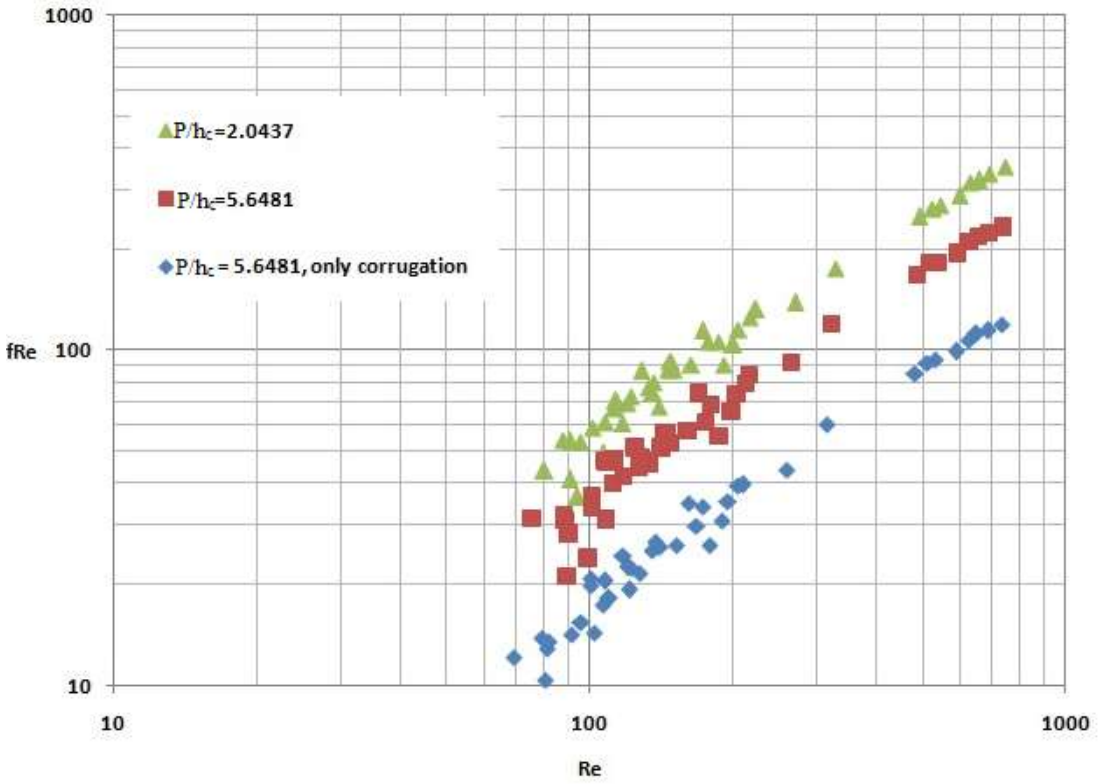

Fig. 18: Effect of corrugation pitch on friction factor: corrugation angle = 30°, q = 1.63 (AC+HST)

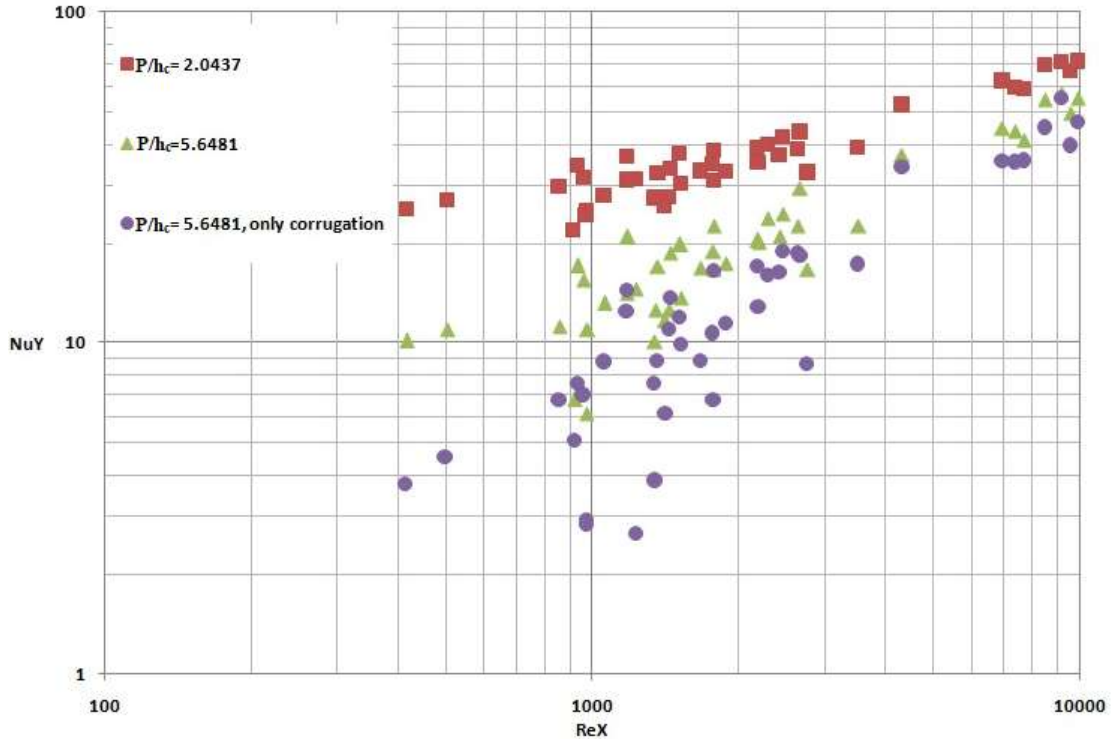

Fig. 19: Effect of corrugation pitch on Nusselt number: corrugation angle = 30°, q = 1.63 (AC+HST)

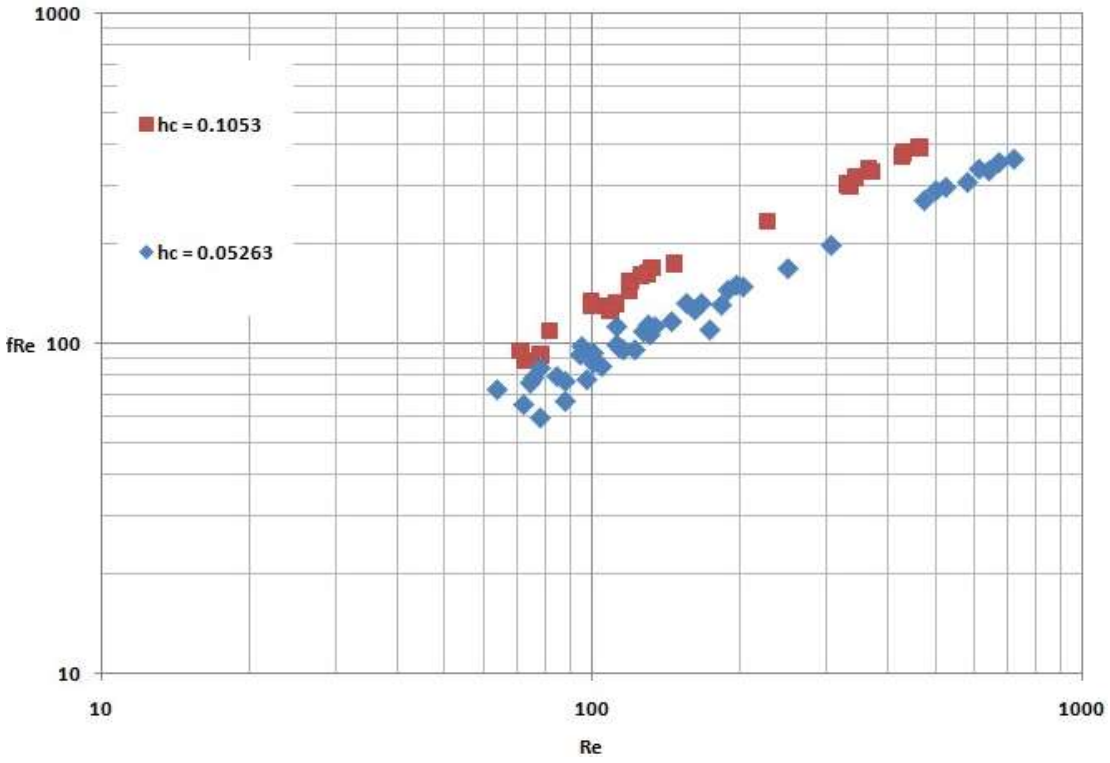

Fig. 20: Effect of corrugation height, y = 2.5, t_{hl} = 0.1053, θ = 60°, α = 30° (friction factor) (SC+TTOT)

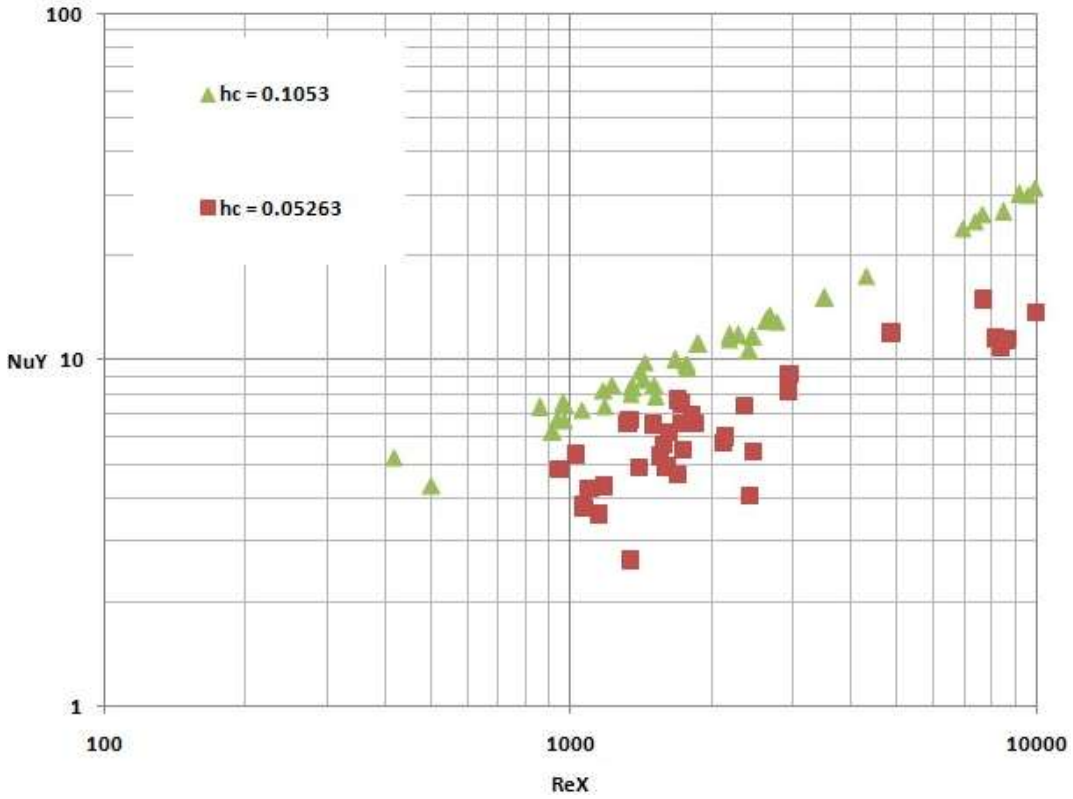

Fig. 21: Effect of corrugation height, y = 2.5, t_{hl} = 0.1053, θ = 60°, α = 30° (Nusselt number) (SC+TTOT)

The increase in Nusselt number and friction factor with different geometrical parameters (excluding pitch) of wire coil, corrugation, screw tape, twisted tape and the duct can be rationally explained by the following facts. As the values of the geometrical parameters of the inserts increase, the insert surface area increases and both the thickness of hydrodynamic and thermal boundary layer increase due to the increased hydrothermal impedance into the flow. The velocity and temperature profiles become flatter. In the case of using helical screw-tape inserts and twisted-tape inserts individually, only swirl flow is observed. With the addition of wire-coil insert and corrugation, increased fluid mixing is achieved due to boundary layer (both hydrodynamic and thermal) separation, flow reattachment to the channel wall and the surfaces of the inserts and recirculation of flow. Periodic separation and reattachment of the boundary layer are more frequent due to the inertia forces generated by the helical screw tape and twisted tape. On the other hand, increased pressure loss due to momentum loss is observed along with increased heat transfer due to an increase in both momentum and thermal diffusion at molecular level as well as at macroscopic bulk flow level. The performance of all other compound techniques is also noted to be better than that of the individual inserts. The developed correlations and performance evaluation show that the combined geometry in case of all the compound enhancement techniques performed significantly (55 % to 79 % increase in heat duty at constant pumping power) and (23 % to 39 % reduction in pumping power at constant heat duty) better than individual fins.

4. Correlations developed for compound techniques

From the phenomenological point of view, the associated thermo-fluid dynamics of the present investigation concerns buoyancy force, flow development length, inertia force,

thermal diffusivity vis-a-vis momentum diffusivity, thermal correction effect of the viscosity and all other geometrical parameters. All these effects are adequately taken care of and captured by non-dimensional parameters while setting the building blocks of the correlations and giving the correlations tentative structural forms.

Correlations are developed for Nusselt number and friction factor for a combination of inserts. Experimental data are fitted by log-linear regression analysis. The correlations are given a general structure and the experimental data agree with the prediction from correlations generally within ± 20 % for 80 % - 90 % data. The deviation of friction factor and Nusselt number correlation data from experimental data is shown in Figure 22 and Figure 23 respectively.

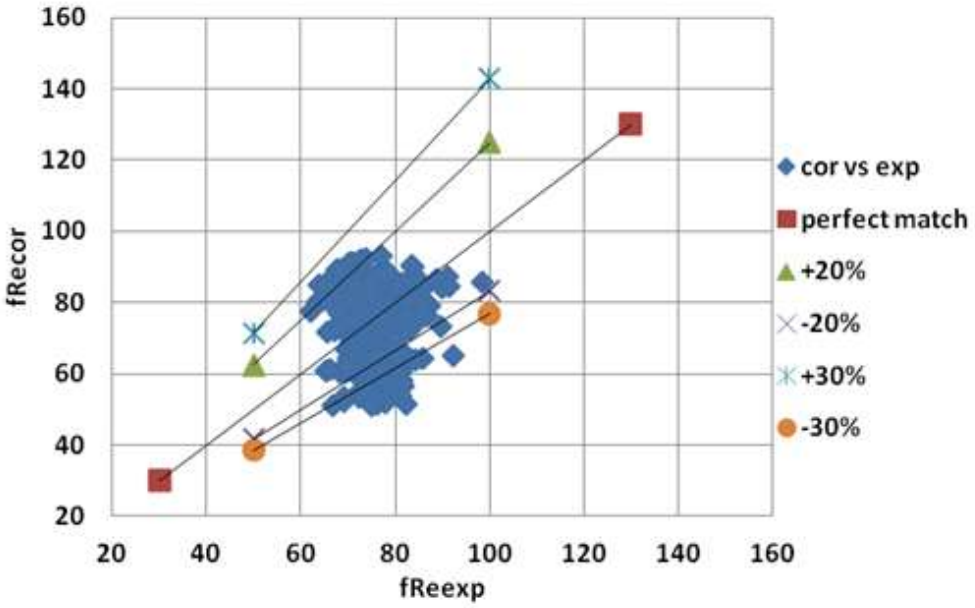

Fig. 22: Pressure drop data, experimental vs. correlation for SC and HST

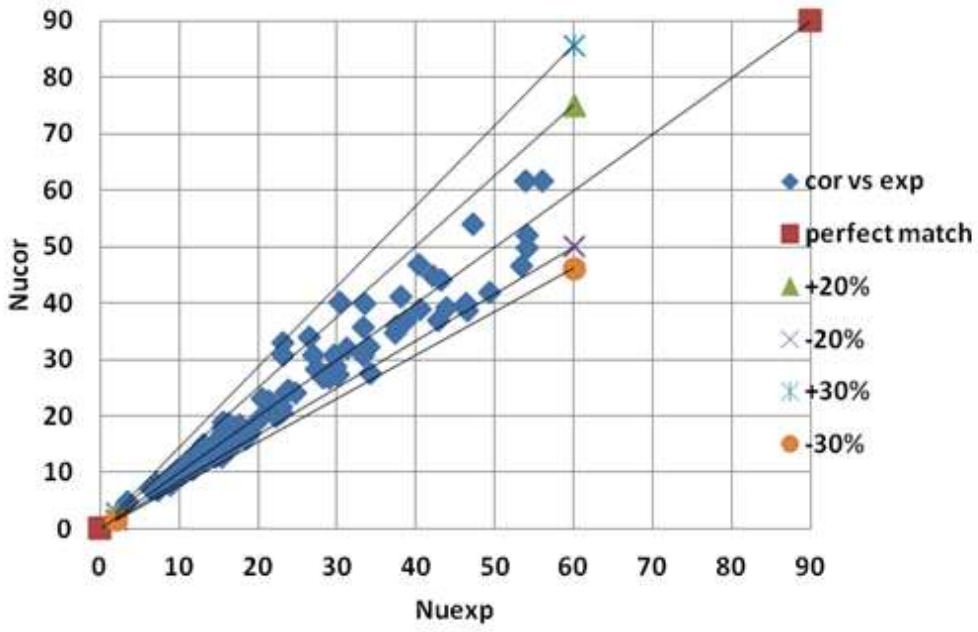

Fig. 23: Heat transfer data, experimental vs. correlation for SC and HST

Nusselt number correlation for combination of helical screw-tape inserts and wire-coil inserts:

$$Nu = 5.172 Gz^{0.269} \mathrm{Re}^{0.251} \mathrm{Pr}^{0.266} Gr^{0.277} q^{0.276} t_{hl}^{0.275} (\sin\theta)^{0.244} (\sin\delta)^{0.239} d_{star}^{0.223} \left(\frac{\mu_b}{\mu_w}\right)^{0.14} \left(\frac{1}{AR} + 0.1\right)^{0.153} \quad (1)$$

Friction factor correlation for combination of helical screw-tape inserts and wire-coil inserts:

$$f\,\mathrm{Re} = 19.111 \mathrm{Re}^{0.291} q^{0.3325} t_{hl}^{0.112} (\sin\theta)^{0.282} (\sin\delta)^{0.121} d_{star}^{0.204} (AR)^{-1.235} \quad (2)$$

Nusselt number correlation for WCI+HST combination

$$Nu = 5.174\left[\begin{array}{l}\left(\left(1+0.07156Gz^{0.88}\right)^{2.56}+8.45\times10^{-6}\left(Sw.\mathrm{Pr}^{0.555}\right)^{2.663}\right)^{2}+\\ 1.50525\times10^{-15}(\mathrm{Re}_{ax}\,Ra)^{2.16}\end{array}\right]^{0.1}$$
$$\times\left(\frac{\mu_b}{\mu_w}\right)^{0.14}\left(\frac{1}{AR}+0.1\right)^{0.153}\times\left(1+\frac{\left(1+\exp(0.08922q)\right)\times\exp(0.087499\sin\delta)}{(d_{star})^{0.6458}}\right) \quad (3)$$

Friction factor correlation for WCI+HST combination

$$f\,\mathrm{Re} = 17.342\left(\frac{\pi+2-\frac{2t}{D_h}}{\left(\frac{\pi-4t}{D_h}\right)}\right)\left(1+10^{-6}\,Sw^{2.6801}\right)^{0.141}\times$$
$$\left(1+\frac{\left(1+\exp(0.083q)\right)\times\exp(0.05786987\sin\delta)}{(d_{star})^{0.625754}}\right)(AR)^{-1.235} \quad (4)$$

Correlation for Nusselt number for combined experiment (axial corrugation and screw-tape insert)

$$Nu = 5.173\left[\begin{array}{l}\left(\left(1+0.07156Gz^{0.88}\right)^{2.56}+8.45\times10^{-6}\left(Sw.\mathrm{Pr}^{0.555}\right)^{2.663}\right)^{2}+1.50525\times\\ 10^{-15}(\mathrm{Re}_{ax}\,Ra)^{2.16}\end{array}\right]^{0.1}$$
$$\times\left(\frac{\mu_b}{\mu_w}\right)^{0.14}\left(\frac{1}{AR}+0.1\right)^{0.153}\times\left(1+\frac{\left(1+\exp(0.08922q)\right)\times\exp(0.087499\sin\alpha)}{\left(\frac{P}{h_c}\right)^{0.6458}}\right) \quad (5)$$

Correlation for predicting friction factor for combined axial corrugation and screw-tape insert is given by:

$$f\,\mathrm{Re} = 17.35\left(\frac{\pi + 2 - \frac{2t}{D_h}}{\left(\frac{\pi - 4t}{D_h}\right)}\right)\left(1 + 10^{-6}\,Sw^{2.6801}\right)^{0.141} \times$$

$$\left(1 + \frac{\left(1 + \exp(0.083q)\right) \times \exp(0.05786987 \sin\alpha)}{\left(\frac{P}{h_c}\right)^{0.625754}}\right)(AR)^{-1.235} \tag{6}$$

Correlation for Nusselt number for combined experiment (helical corrugation and screw-tape insert):

$$Nu = 5.173\left[\left(\left(1 + 0.07156Gz^{0.88}\right)^{2.56} + 8.45 \times 10^{-6}\left(Sw.\mathrm{Pr}^{0.555}\right)^{2.663}\right)^{2} + 1.50525 \times 10^{-15}(\mathrm{Re}_{ax}\,Ra)^{2.16}\right]^{0.1}$$

$$\times\left(\frac{\mu_b}{\mu_w}\right)^{0.14}\left(\frac{1}{AR} + 0.1\right)^{0.153} \times \left(1 + \frac{\left(1 + \exp(0.08922q)\right) \times \exp(0.087499 \sin\alpha)}{\left(\frac{P}{h_c}\right)^{0.6458}}\right) \tag{7}$$

Correlation for predicting friction factor for combined helical corrugation and screw-tape insert is given by:

$$f\,\mathrm{Re} = 17.35\left(\frac{\pi + 2 - \frac{2t}{D_h}}{\left(\frac{\pi - 4t}{D_h}\right)}\right)\left(1 + 10^{-6}\,Sw^{2.6801}\right)^{0.141} \times$$

$$\left(1 + \frac{\left(1 + \exp(0.083q)\right) \times \exp(0.05786987 \sin\alpha)}{\left(\frac{P}{h_c}\right)^{0.625754}}\right)(AR)^{-1.235} \tag{8}$$

Correlation for predicting Nusselt number for combined twisted-tape insert with oblique teeth and integral spiral corrugation roughness elements:

$$Nu = 5.171 Gz^{0.352} (\mathrm{Re})^{0.135} \mathrm{Pr}^{0.204} Gr^{-0.144} h_c^{0.0382} t_{hl}^{0.0705} (\sin\theta)^{0.126} (\sin\alpha)^{-0.368} \times \left(\frac{\mu_b}{\mu_w}\right)^{0.14} \left(\frac{1}{AR} + 0.1\right)^{0.153} \quad (9)$$

Correlation for predicting friction factor for combined twisted-tape with oblique teeth and integral spiral corrugation roughness elements:

$$f\,\mathrm{Re} = 17.355 \left(\frac{\mathrm{Re}}{\sqrt{y}}\right)^{0.435} t_{hl}^{-0.0707} (\sin\theta)^{-0.376} h_c^{-0.821} (\sin\alpha)^{-0.101} (AR)^{-1.235} \quad (10)$$

5. PERFORMANCE EVALUATION

The performance of the fin geometry is evaluated by two standard methods [41],

P_1 = (combined enhanced geometry/individual-enhanced geometry), for increased heat transfer and fixed pumping power.

P_2 = (combined enhanced geometry/individual-enhanced geometry) for constant heat duty and reduced pumping power.

$R_1 > 1$ and $R_2 < 1$ are for useful fin geometry and recommended for use in the industry.

Table 1 and Table 2 show the only combined performance of wire-coil insert and helical screw-tape insert with oblique teeth. The combined enhancement fins yield (as shown in Table 1) 55 % to 79 % increased heat duty at constant pumping power compared to the individual enhancement fins. Also, Table 2 shows decrease of 23 % to 39% reduction in pumping power at constant heat duty. Similar tables were obtained for other compound techniques used in the study. For brevity and paucity in journal space, these are not furnished here.

Table 1: Performance evaluation table [P_1 : δ = 30° (1) and 60° (2) d_{star} = 0.07692 (1) and 0.0526 (2)] (WCI+HSTOT)

AR 1.0								
				P_1				
	R2R2		**R1R2**		**R2R1**		**R1R1**	
q = ∞, t_{hl} = 0.0769, γ = 30°, δ = 30°, dstar = 0.07692	P_{R1R1}	P_{R1R2}	P_{R1R1}	P_{R1R2}	P_{R1R1}	P_{R1R2}	P_{R1R1}	P_{R1R2}
	1.660	**1.676**	**1.697**	**1.711**	**1.730**	**1.752**	**1.770**	**1.789**
q = 1.0256, t_{hl} = 0.1154, γ = 45°, δ = 30°, dstar = 0.07692	P_{R1R1}	P_{R1R2}	P_{R1R1}	P_{R1R2}	P_{R1R1}	P_{R1R2}	P_{R1R1}	P_{R1R2}
	1.666	**1.674**	**1.688**	**1.694**	**1.705**	**1.724**	**1.734**	**1.747**
q = 0.769, t_{hl} = 0.1538, γ = 45°, δ = 45°, dstar = 0.07692	P_{R1R1}	P_{R1R2}	P_{R1R1}	P_{R1R2}	P_{R1R1}	P_{R1R2}	P_{R1R1}	P_{R1R2}
	1.554	**1.557**	**1.575**	**1.589**	**1.599**	**1.621**	**1.626**	**1.641**
q = ∞, t_{hl} = 0.0625, γ = 30°, δ = 45°, dstar = 0.0625	P_{R1R1}	P_{R1R2}	P_{R1R1}	P_{R1R2}	P_{R1R1}	P_{R1R2}	P_{R1R1}	P_{R1R2}
	1.597	**1.608**	**1.618**	**1.623**	**1.631**	**1.641**	**1.647**	**1.658**
q = 1.3333, t_{hl} = 0.09575, γ = 45°, δ = 45°, dstar = 0.0625	P_{R1R1}	P_{R1R2}	P_{R1R1}	P_{R1R2}	P_{R1R1}	P_{R1R2}	P_{R1R1}	P_{R1R2}
	1.700	**1.712**	**1.715**	**1.717**	**1.723**	**1.744**	**1.745**	**1.769**
q = 1, t_{hl} = 0.125, γ = 60°, δ = 45°, dstar = 0.0625	P_{R1R1}	P_{R1R2}	P_{R1R1}	P_{R1R2}	P_{R1R1}	P_{R1R2}	P_{R1R1}	P_{R1R2}
	1.584	**1.603**	**1.625**	**1.646**	**1.656**	**1.657**	**1.658**	**1.676**
q = ∞, t_{hl} = 0.0526, γ = 30°, δ = 60°, dstar = 0.0526	P_{R1R1}	P_{R1R2}	P_{R1R1}	P_{R1R2}	P_{R1R1}	P_{R1R2}	P_{R1R1}	P_{R1R2}
	1.534	**1.548**	**1.562**	**1.578**	**1.579**	**1.589**	**1.598**	**1.617**
q = 1.5438, t_{hl} = 0.0789, γ = 45°, δ = 60°, dstar = 0.0526	P_{R1R1}	P_{R1R2}	P_{R1R1}	P_{R1R2}	P_{R1R1}	P_{R1R2}	P_{R1R1}	P_{R1R2}
	1.622	**1.625**	**1.647**	**1.648**	**1.659**	**1.659**	**1.665**	**1.687**
q = 1.15789, t_{hl} = 0.10526, γ = 45°, δ = 45°, dstar = 0.0526	P_{R1R1}	P_{R1R2}	P_{R1R1}	P_{R1R2}	P_{R1R1}	P_{R1R2}	P_{R1R1}	P_{R1R2}
	1.635	**1.656**	**1.669**	**1.669**	**1.689**	**1.690**	**1.715**	**1.730**
AR 0.5								
				P_1				
	R2R2		**R1R2**		**R2R1**		**R1R1**	
q = ∞, t_{hl} = 0.0769, γ = 30°, δ = 30°, dstar = 0.07692	P_{R1R1}	P_{R1R2}	P_{R1R1}	P_{R1R2}	P_{R1R1}	P_{R1R2}	P_{R1R1}	P_{R1R2}
	1.652	**1.673**	**1.681**	**1.682**	**1.690**	**1.709**	**1.722**	**1.744**
q = 1.0256, t_{hl} = 0.1154, γ = 45°, δ = 30°, dstar = 0.07692	P_{R1R1}	P_{R1R2}	P_{R1R1}	P_{R1R2}	P_{R1R1}	P_{R1R2}	P_{R1R1}	P_{R1R2}

	1.653	**1.654**	**1.679**	**1.698**	**1.710**	**1.730**	**1.754**	**1.778**
q = 0.769, t_{hl} = 0.1538, γ = 45º, δ = 45º, dstar = 0.07692	P_{R1R1}	P_{R1R2}	P_{R1R1}	P_{R1R2}	P_{R1R1}	P_{R1R2}	P_{R1R1}	P_{R1R2}
	1.551	**1.566**	**1.591**	**1.603**	**1.626**	**1.637**	**1.657**	**1.680**
q = ∞, t_{hl} = 0.0625, γ = 30º, δ = 45º, dstar = 0.0625	P_{R1R1}	P_{R1R2}	P_{R1R1}	P_{R1R2}	P_{R1R1}	P_{R1R2}	P_{R1R1}	P_{R1R2}
	1.612	**1.625**	**1.634**	**1.649**	**1.673**	**1.682**	**1.685**	**1.697**
q = 1.3333, t_{hl} = 0.09575, γ = 45º, δ = 45º, dstar = 0.0625	P_{R1R1}	P_{R1R2}	P_{R1R1}	P_{R1R2}	P_{R1R1}	P_{R1R2}	P_{R1R1}	P_{R1R2}
	1.721	**1.742**	**1.765**	**1.785**	**1.795**	**1.806**	**1.830**	**1.837**
q = 1, t_{hl} = 0.125, γ = 60º, δ = 45º, dstar = 0.0625	P_{R1R1}	P_{R1R2}	P_{R1R1}	P_{R1R2}	P_{R1R1}	P_{R1R2}	P_{R1R1}	P_{R1R2}
	1.586	**1.603**	**1.617**	**1.635**	**1.637**	**1.654**	**1.659**	**1.669**
q = ∞, t_{hl} = 0.0526, γ = 30º, δ = 60º, dstar = 0.0526	P_{R1R1}	P_{R1R2}	P_{R1R1}	P_{R1R2}	P_{R1R1}	P_{R1R2}	P_{R1R1}	P_{R1R2}
	1.543	**1.559**	**1.563**	**1.564**	**1.577**	**1.579**	**1.598**	**1.598**
q = 1.5438, t_{hl} = 0.0789, γ = 45º, δ = 60º, dstar = 0.0526	P_{R1R1}	P_{R1R2}	P_{R1R1}	P_{R1R2}	P_{R1R1}	P_{R1R2}	P_{R1R1}	P_{R1R2}
	1.625	**1.638**	**1.659**	**1.680**	**1.696**	**1.700**	**1.716**	**1.738**
q = 1.15789, t_{hl} = 0.10526, γ = 45º, δ = 45º, dstar = 0.0526	P_{R1R1}	P_{R1R2}	P_{R1R1}	P_{R1R2}	P_{R1R1}	P_{R1R2}	P_{R1R1}	P_{R1R2}
	1.628	**1.633**	**1.650**	**1.660**	**1.672**	**1.687**	**1.688**	**1.689**
AR 0.33								
				P_1				
	R2R2		**R1R2**		**R2R1**		**R1R1**	
q = ∞, t_{hl} = 0.0769, γ = 30º, δ = 30º, dstar = 0.07692	P_{R1R1}	P_{R1R2}	P_{R1R1}	P_{R1R2}	P_{R1R1}	P_{R1R2}	P_{R1R1}	P_{R1R2}
	1.667	**1.684**	**1.685**	**1.693**	**1.713**	**1.731**	**1.748**	**1.762**
q = 1.0256, t_{hl} = 0.1154, γ = 45º, δ = 30º, dstar = 0.07692	P_{R1R1}	P_{R1R2}	P_{R1R1}	P_{R1R2}	P_{R1R1}	P_{R1R2}	P_{R1R1}	P_{R1R2}
	1.666	**1.689**	**1.707**	**1.725**	**1.742**	**1.763**	**1.787**	**1.794**
q = 0.769, t_{hl} = 0.1538, γ = 45º, δ = 45º, dstar = 0.07692	P_{R1R1}	P_{R1R2}	P_{R1R1}	P_{R1R2}	P_{R1R1}	P_{R1R2}	P_{R1R1}	P_{R1R2}
	1.559	**1.582**	**1.596**	**1.601**	**1.620**	**1.636**	**1.644**	**1.664**
q = ∞, t_{hl} = 0.0625, γ = 30º, δ = 45º, dstar = 0.0625	P_{R1R1}	P_{R1R2}	P_{R1R1}	P_{R1R2}	P_{R1R1}	P_{R1R2}	P_{R1R1}	P_{R1R2}
	1.620	**1.639**	**1.658**	**1.681**	**1.687**	**1.691**	**1.711**	**1.736**
q = 1.3333, t_{hl} = 0.09575, γ = 45º, δ = 45º, dstar = 0.0625	P_{R1R1}	P_{R1R2}	P_{R1R1}	P_{R1R2}	P_{R1R1}	P_{R1R2}	P_{R1R1}	P_{R1R2}

	1.696	**1.712**	**1.723**	**1.732**	**1.749**	**1.763**	**1.787**	**1.787**
q = 1, t_{hl} = 0.125, γ = 60º, δ = 45º, dstar = 0.0625	P_{R1R1}	P_{R1R2}	P_{R1R1}	P_{R1R2}	P_{R1R1}	P_{R1R2}	P_{R1R1}	P_{R1R2}
	1.579	**1.584**	**1.592**	**1.599**	**1.619**	**1.623**	**1.625**	**1.644**
q = ∞, t_{hl} = 0.0526, γ = 30º, δ = 60º, dstar = 0.0526	P_{R1R1}	P_{R1R2}	P_{R1R1}	P_{R1R2}	P_{R1R1}	P_{R1R2}	P_{R1R1}	P_{R1R2}
	1.555	**1.563**	**1.567**	**1.580**	**1.583**	**1.603**	**1.614**	**1.619**
q = 1.5438, t_{hl} = 0.0789, γ = 45º, δ = 60º, dstar = 0.0526	P_{R1R1}	P_{R1R2}	P_{R1R1}	P_{R1R2}	P_{R1R1}	P_{R1R2}	P_{R1R1}	P_{R1R2}
	1.604	**1.625**	**1.638**	**1.652**	**1.655**	**1.674**	**1.676**	**1.697**
q = 1.15789, t_{hl} = 0.10526, γ = 45º, δ = 45º, dstar = 0.0526	P_{R1R1}	P_{R1R2}	P_{R1R1}	P_{R1R2}	P_{R1R1}	P_{R1R2}	P_{R1R1}	P_{R1R2}
	1.634	**1.646**	**1.663**	**1.667**	**1.682**	**1.688**	**1.698**	**1.709**

Table 2: Performance evaluation table [P_2: δ = 30° (1) and 60° (2) d_{star} = 0.07692 (1) and 0.0526 (2)] (WCI+HSTOT)

AR 1.0								
				P_2				
	R2R2		**R1R2**		**R2R1**		**R1R1**	
q = ∞, t_{hl} = 0.0769, γ = 30°, δ = 30°, dstar = 0.07692	P_{R2R1}	P_{R2R2}	P_{R2R1}	P_{R2R2}	P_{R2R1}	P_{R2R2}	P_{R2R1}	P_{R2R2}
	0.766	**0.768**	**0.770**	**0.772**	**0.774**	**0.775**	**0.778**	**0.778**
q = 1.0256, t_{hl} = 0.1154, γ = 45°, δ = 30°, dstar = 0.07692	P_{R2R1}	P_{R2R2}	P_{R2R1}	P_{R2R2}	P_{R2R1}	P_{R2R2}	P_{R2R1}	P_{R2R2}
	0.768	**0.769**	**0.771**	**0.772**	**0.772**	**0.773**	**0.775**	**0.776**
q = 0.769, t_{hl} = 0.1538, γ = 45°, δ = 45°, dstar = 0.07692	P_{R2R1}	P_{R2R2}	P_{R2R1}	P_{R2R2}	P_{R2R1}	P_{R2R2}	P_{R2R1}	P_{R2R2}
	0.750	**0.751**	**0.754**	**0.755**	**0.757**	**0.759**	**0.761**	**0.761**
q = ∞, t_{hl} = 0.0625, γ = 30°, δ = 45°, dstar = 0.0625	P_{R2R1}	P_{R2R2}	P_{R2R1}	P_{R2R2}	P_{R2R1}	P_{R2R2}	P_{R2R1}	P_{R2R2}
	0.674	**0.676**	**0.678**	**0.680**	**0.681**	**0.682**	**0.683**	**0.685**
q = 1.3333, t_{hl} = 0.09575, γ = 45°, δ = 45°, dstar = 0.0625	P_{R2R1}	P_{R2R2}	P_{R2R1}	P_{R2R2}	P_{R2R1}	P_{R2R2}	P_{R2R1}	P_{R2R2}
	0.685	**0.685**	**0.686**	**0.688**	**0.689**	**0.691**	**0.693**	**0.696**
q = 1, t_{hl} = 0.125, γ = 60°, δ = 45°, dstar = 0.0625	P_{R2R1}	P_{R2R2}	P_{R2R1}	P_{R2R2}	P_{R2R1}	P_{R2R2}	P_{R2R1}	P_{R2R2}
	0.663	**0.665**	**0.666**	**0.667**	**0.668**	**0.670**	**0.670**	**0.671**
q = ∞, t_{hl} = 0.0526, γ = 30°, δ = 60°, dstar = 0.0526	P_{R2R1}	P_{R2R2}	P_{R2R1}	P_{R2R2}	P_{R2R1}	P_{R2R2}	P_{R2R1}	P_{R2R2}
	0.688	**0.689**	**0.690**	**0.691**	**0.693**	**0.695**	**0.696**	**0.698**
q = 1.5438, t_{hl} = 0.0789, γ = 45°, δ = 60°, dstar = 0.0526	P_{R2R1}	P_{R2R2}	P_{R2R1}	P_{R2R2}	P_{R2R1}	P_{R2R2}	P_{R2R1}	P_{R2R2}
	0.615	**0.615**	**0.617**	**0.618**	**0.619**	**0.620**	**0.622**	**0.622**
q = 1.15789, t_{hl} = 0.10526, γ = 45°, δ = 45°, dstar = 0.0526	P_{R2R1}	P_{R2R2}	P_{R2R1}	P_{R2R2}	P_{R2R1}	P_{R2R2}	P_{R2R1}	P_{R2R2}
	0.633	**0.633**	**0.635**	**0.636**	**0.637**	**0.640**	**0.641**	**0.644**
AR 0.5								
				P_2				
	R2R2		**R1R2**		**R2R1**		**R1R1**	
q = ∞, t_{hl} = 0.0769, γ = 30°, δ = 30°, dstar = 0.07692	P_{R2R1}	P_{R2R2}	P_{R2R1}	P_{R2R2}	P_{R2R1}	P_{R2R2}	P_{R2R1}	P_{R2R2}
	0.767	**0.770**	**0.772**	**0.773**	**0.773**	**0.775**	**0.776**	**0.777**
q = 1.0256, t_{hl} = 0.1154, γ = 45°, δ = 30°, dstar = 0.07692	P_{R2R1}	P_{R2R2}	P_{R2R1}	P_{R2R2}	P_{R2R1}	P_{R2R2}	P_{R2R1}	P_{R2R2}

	0.768	**0.768**	**0.770**	**0.771**	**0.772**	**0.774**	**0.777**	**0.778**
q = 0.769, t_{hl} = 0.1538, γ = 45º, δ = 45º, dstar = 0.07692	P_{R2R1}	P_{R2R2}	P_{R2R1}	P_{R2R2}	P_{R2R1}	P_{R2R2}	P_{R2R1}	P_{R2R2}
	0.750	**0.752**	**0.754**	**0.756**	**0.757**	**0.757**	**0.758**	**0.758**
q = ∞, t_{hl} = 0.0625, γ = 30º, δ = 45º, dstar = 0.0625	P_{R2R1}	P_{R2R2}	P_{R2R1}	P_{R2R2}	P_{R2R1}	P_{R2R2}	P_{R2R1}	P_{R2R2}
	0.674	**0.675**	**0.676**	**0.677**	**0.679**	**0.681**	**0.682**	**0.684**
q = 1.3333, t_{hl} = 0.09575, γ = 45º, δ = 45º, dstar = 0.0625	P_{R2R1}	P_{R2R2}	P_{R2R1}	P_{R2R2}	P_{R2R1}	P_{R2R2}	P_{R2R1}	P_{R2R2}
	0.685	**0.687**	**0.687**	**0.689**	**0.690**	**0.691**	**0.693**	**0.695**
q = 1, t_{hl} = 0.125, γ = 60º, δ = 45º, dstar = 0.0625	P_{R2R1}	P_{R2R2}	P_{R2R1}	P_{R2R2}	P_{R2R1}	P_{R2R2}	P_{R2R1}	P_{R2R2}
	0.663	**0.665**	**0.666**	**0.668**	**0.669**	**0.670**	**0.670**	**0.672**
q = ∞, t_{hl} = 0.0526, γ = 30º, δ = 60º, dstar = 0.0526	P_{R2R1}	P_{R2R2}	P_{R2R1}	P_{R2R2}	P_{R2R1}	P_{R2R2}	P_{R2R1}	P_{R2R2}
	0.688	**0.691**	**0.692**	**0.694**	**0.696**	**0.698**	**0.699**	**0.702**
q = 1.5438, t_{hl} = 0.0789, γ = 45º, δ = 60º, dstar = 0.0526	P_{R2R1}	P_{R2R2}	P_{R2R1}	P_{R2R2}	P_{R2R1}	P_{R2R2}	P_{R2R1}	P_{R2R2}
	0.616	**0.618**	**0.620**	**0.620**	**0.622**	**0.624**	**0.624**	**0.626**
q = 1.15789, t_{hl} = 0.10526, γ = 45º, δ = 45º, dstar = 0.0526	P_{R2R1}	P_{R2R2}	P_{R2R1}	P_{R2R2}	P_{R2R1}	P_{R2R2}	P_{R2R1}	P_{R2R2}
	0.634	**0.634**	**0.635**	**0.635**	**0.637**	**0.639**	**0.639**	**0.641**
AR 0.33								
				P_2				
	R2R2		**R1R2**		**R2R1**		**R1R1**	
q = ∞, t_{hl}= 0.0769, γ = 30º, δ = 30º, dstar = 0.07692	P_{R2R1}	P_{R2R2}	P_{R2R1}	P_{R2R2}	P_{R2R1}	P_{R2R2}	P_{R2R1}	P_{R2R2}
	0.766	**0.767**	**0.769**	**0.771**	**0.771**	**0.772**	**0.773**	**0.774**
q = 1.0256, t_{hl}= 0.1154, γ = 45º, δ = 30º, dstar = 0.07692	P_{R2R1}	P_{R2R2}	P_{R2R1}	P_{R2R2}	P_{R2R1}	P_{R2R2}	P_{R2R1}	P_{R2R2}
hl	**0.766**	**0.769**	**0.769**	**0.771**	**0.772**	**0.772**	**0.772**	**0.773**
q = 0.769, t_{hl}= 0.1538, γ = 45º, δ = 45º, dstar = 0.07692	P_{R2R1}	P_{R2R2}	P_{R2R1}	P_{R2R2}	P_{R2R1}	P_{R2R2}	P_{R2R1}	P_{R2R2}
	0.752	**0.754**	**0.755**	**0.757**	**0.759**	**0.759**	**0.760**	**0.762**
q = ∞, t_{hl}= 0.0625, γ = 30º, δ = 45º, dstar = 0.0625	P_{R2R1}	P_{R2R2}	P_{R2R1}	P_{R2R2}	P_{R2R1}	P_{R2R2}	P_{R2R1}	P_{R2R2}
	0.675	**0.675**	**0.675**	**0.677**	**0.679**	**0.680**	**0.682**	**0.684**
q = 1.3333, t_{hl} = 0.09575, γ = 45º, δ = 45º, dstar = 0.0625	P_{R2R1}	P_{R2R2}	P_{R2R1}	P_{R2R2}	P_{R2R1}	P_{R2R2}	P_{R2R1}	P_{R2R2}
	0.687	**0.688**	**0.690**	**0.692**	**0.694**	**0.694**	**0.694**	**0.694**
q = 1, t_{hl} = 0.125, γ = 60º,	P_{R2R1}	P_{R2R2}	P_{R2R1}	P_{R2R2}	P_{R2R1}	P_{R2R2}	P_{R2R1}	P_{R2R2}

δ = 45º, dstar = 0.0625								
	0.665	**0.666**	**0.668**	**0.670**	**0.672**	**0.672**	**0.674**	**0.675**
q = ∞, t_{hl} = 0.0526, γ = 30º, δ = 60º, dstar = 0.0526	P_{R2R1}	P_{R2R2}	P_{R2R1}	P_{R2R2}	P_{R2R1}	P_{R2R2}	P_{R2R1}	P_{R2R2}
	0.689	**0.689**	**0.691**	**0.693**	**0.695**	**0.696**	**0.697**	**0.700**
q = 1.5438, t_{hl} = 0.0789, γ = 45º, δ = 60º, dstar = 0.0526	P_{R2R1}	P_{R2R2}	P_{R2R1}	P_{R2R2}	P_{R2R1}	P_{R2R2}	P_{R2R1}	P_{R2R2}
	0.616	**0.617**	**0.619**	**0.622**	**0.622**	**0.623**	**0.624**	**0.625**
q = 1.15789, t_{hl} = 0.10526, γ = 45º, δ = 45º, dstar = 0.0526	P_{R2R1}	P_{R2R2}	P_{R2R1}	P_{R2R2}	P_{R2R1}	P_{R2R2}	P_{R2R1}	P_{R2R2}
	0.634	**0.636**	**0.638**	**0.640**	**0.642**	**0.643**	**0.643**	**0.644**

6. CONCLUSIONS

The heat transfer and pressure drop characteristics of laminar duct flow using five different types of compound inserts were studied and the following conclusions were drawn:

- Friction factor and Nusselt number increased with Reynolds number, aspect ratio of the channel, helix angle and diameter of the wire coil.
- The maximum and minimum values were obtained for channels having AR=1 and AR=0.33 respectively for both friction factor and Nusselt number.
- The wire-coil insert having 60° and 30° helix angles gave maximum and minimum friction factor and Nusselt number.
- The wire coil having 0.07692 and 0.0526 dimensionless diameter showed maximum and minimum friction factor and Nusselt number.
- An increase in tooth angle and tooth horizontal length on the screw-tape insert and twisted-tape insert increased Nusselt number and friction factor.
- The tape with 30º tooth angle showed minimum Nusselt number and friction factor and the tape with 60º tooth angle showed maximum values.

- The friction factor and Nusselt number were also found to increase with the corrugation angle and corrugation height. The effect of corrugation pitch was the reverse.
- An increase in heat duty of 55 % to 79 % at constant pumping power and a 23 % to 39 % reduction in pumping power at constant heat duty were observed for combined inserts over those for individual inserts in the case of all the compound techniques used in the study.
- The compound inserts were found to be effective because the increase in Nusselt number was more significant than the increase in friction factor.
- All the observations were adequately explained phenomenologically.

ACKNOWLEDGEMENT

Financial support for the current research from AICTE [20/AICTE/RIFD/RPS (Policy II): 84/2012-2013]; UGC [UGC 41-989/2012 (SR)]; DST [SR/S3/MERC-0045/2010(G)]; CSIR [22(0386)/05/EMR-II] and the Government of India is gratefully acknowledged.

NOMENCLATURE

A	Heat transfer area
AR	Aspect ratio
A_c	Axial flow cross-sectional area
A_o	Plain duct flow cross-sectional area
C	Screw-tape centre clearance, m
d_c	Wire-coil diameter, m

d	Rod diameter for helical screw tape, m
D_h	Hydraulic diameter of the test section, m
H	Pitch of the tape for 180º rotation
h_c	Corrugation height, m
P	Corrugation pitch, m, Performance ratio, dimensionless
t	Tape thickness, m
t_{hl}^*	Tooth horizontal length, m
V_a	Mean axial velocity = $\dot{m}/\rho A_c$, m/s
V_s	Actual swirl velocity at duct wall = $V_a\left[1+\left(\pi/2y\right)^2\right]^{0.5}$, m/s
W	Width of channel cross-section, m

Greek Symbols

α	Corrugation helix angle
δ	Helix angle of the wire coil
θ	Oblique teeth angle on screw-tape insert
ρ	Density of the fluid, kg/m^3
μ	Fluid dynamic viscosity, kg/ms

Subscripts

ax	at axial flow condition
b	at bulk fluid temperature
w	at duct wall temperature

Non-dimensional Numbers

c	Dimensionless screw-tape centre clearance [C/ D_h]
d_{star}	Dimensionless wire-coil diameter [d_c/ D_h]
f	Fanning Friction factor
Gr	Grashof number, dimensionless
Gz	Graetz number, dimensionless
Nu	Nusselt number
Pr	Prandtl number
Q	Wc/d
q	Q/D_h
Re	Reynolds number
Re_{ax}	Reynolds number based on axial velocity = $(\rho V_a D_h)/\mu$
Re_{sw}	Reynolds number based on swirl velocity = $(\rho V_s D_h)/\mu$

Sw Swirl parameter,

$$\frac{\mathrm{Re}_{sw}}{\sqrt{y}} = \left(\frac{\mathrm{Re}}{\sqrt{y}}\right)\left(\frac{\pi}{\left(\pi - 4t/D_h\right)}\right)\left(1+\left(\frac{\pi}{2y}\right)^2\right)^{0.5},$$

t_{hl} Tooth horizontal length on the screw-tape insert

X Pr^n, the value of n depends on the exponent of Pr in the correlation

Y $\left(\frac{\mu_b}{\mu_w}\right)^{-0.14} \times \frac{1}{5.172}$

y Twist ratio, H/D_h

REFERENCES

[1] Webb, R. L., and Kim, N. Y., 2005, "Enhanced heat transfer," Taylor and Francis, NY.

[2] Bergman, T. L., Incropera, F. P., Lavine, A. S., and DeWitt, D. P., 2011, "Introduction to heat transfer," John Wiley & Sons.

[3] Roy, S., and Saha, S. K., 2015, "Thermal and friction characteristics of laminar flow through a circular duct having helical screw-tape with oblique teeth inserts and wire coil inserts," Experimental Thermal and Fluid Science, 68, pp. 733-43. doi.org/10.1016/j.expthermflusci.2015.07.007

[4] Abolarin, S. M., Everts, M. and Meyer, J. P., 2019, "Heat transfer and pressure drop characteristics of alternating clockwise and counter clockwise twisted tape inserts in the transitional flow regime," International Journal of Heat and Mass Transfer, 133, pp. 203-217. doi.org/10.1016/j.ijheatmasstransfer.2018.12.107

[5] Safikhani, Hamed, and Farzad Abbasi, 2015, "Numerical study of nanofluid flow in flat tubes fitted with multiple twisted tapes," Advanced Powder Technology 26(6), pp. 1609-1617. doi.org/10.1016/j.apt.2015.09.002

[6] Qi, C., Liu, M., Luo, T., Pan, Y., and Rao, Z, 2018, "Effects of twisted tape structures on thermo-hydraulic performances of nanofluids in a triangular tube," International Journal of Heat and Mass Transfer, 127, pp. 146-159.
doi.org/10.1016/j.ijheatmasstransfer.2018.08.017

[7] Liu, X., Li, C., Cao, X., Yan, C., and Ding, M, 2018, "Numerical analysis on enhanced performance of new coaxial cross twisted tapes for laminar convective heat transfer," International Journal of Heat and Mass Transfer, 121, pp. 1125-1136. doi.org/10.1016/j.ijheatmasstransfer.2018.01.052

[8] Oliver, D. R., and R. W. J. Aldington, 1986, "Enhancement of laminar flow heat transfer using wire matrix turbulators," Proceedings of the 8th International Heat Transfer Conference, San Fransisco, CA, USA.

[9] Abu-Mulaweh, Hosni I, 2003, "Experimental comparison of heat transfer enhancement methods in heat exchangers," International Journal of Mechanical Engineering Education, 31(2), pp. 160-167. doi.org/10.7227/IJMEE.31.2.8

[10] Chen, Li, and Hong Ji Zhang, 1993, "Convection heat transfer enhancement of oil in a circular tube with spiral spring inserts," ASME-PUBLICATIONS-HTD 249, pp. 45-45.

[11] Sethumadhavan, R., and M. Raja Rao, 1983, "Turbulent flow heat transfer and fluid friction in helical-wire-coil-inserted tubes," International Journal of Heat and Mass Transfer, 26(12), pp. 1833-1845. doi.org/10.1016/S0017-9310(83)80154-9

[12] Herring, Neal R., and Stephen D. Heister, 2009, "On the use of wire-coil inserts to augment tube heat transfer," Journal of Enhanced Heat Transfer 16(1) doi: 10.1615/JEnhHeatTransf.v16.i1.20

[13] Khatua, A. K., Parmanand, K., and Hari, N. S., 2014, "Pressure drop in R-245fa condensation in tubes fitted with coiled-wire inserts," Journal of Enhanced Heat Transfer 21(6) DOI: 10.1615/JEnhHeatTransf.2015012442

[14] Gunes, S., Veysel, O., and Orhan, B., 2010, "Heat transfer enhancement in a tube with equilateral triangle cross sectioned coiled wire inserts," Experimental Thermal and Fluid Science 34(6), pp. 684-691. doi.org/10.1016/j.expthermflusci.2009.12.010

[15] Saraç, B. A., and Bali, T., 2007, "An experimental study on heat transfer and pressure drop characteristics of decaying swirl flow through a circular pipe with a vortex generator," Experimental Thermal and Fluid Science 32(1), pp. 158-165. doi.org/10.1016/j.expthermflusci.2007.03.002

[16] Eiamsa-Ard, S., Thianpong, C., Eiamsa-Ard, P., and Promvonge, P., 2009, "Convective heat transfer in a circular tube with short-length twisted tape insert," International Communications in Heat and Mass Transfer, 36(4), pp. 365-371. doi.org/10.1016/j.icheatmasstransfer.2009.01.006

[17] Sundar, L. S., and Sharma, K. V., 2008, "Experimental investigation of heat transfer and friction factor characteristics in a circular tube with longitudinal strip inserts," Journal of Enhanced Heat Transfer, 15(4).

[18] Uttarwar, S. B., and Raja Rao, M., 1985, "Augmentation of laminar flow heat transfer in tubes by means of wire coil inserts," Journal of Heat Transfer, 107(4), pp. 930-935.

[19] Tiwari, M., and Saha, S. K., 2015, "Laminar flow through a circular tube having transverse ribs and twisted tapes," Journal of Thermal Science and Engineering Applications 7(4), pp. 041009. doi: 10.1115/1.4030792

[20] Garcia, A., Solano, J.P., Vicente, P.G., and Viedma, A., 2007, "Enhancement of laminar and transitional flow heat transfer in tubes by means of wire coil inserts," International Journal of Heat and Mass Transfer, 50(15-16), pp. 3176-3189. doi.org/10.1016/j.ijheatmasstransfer.2007.01.015

[21] Agostini, B., Fabbri, M., Park, J. E., Wojtan, L., Thome, J. R., and Michel, B., 2007, "State of the art of high heat flux cooling technologies," Heat Transfer Engineering, 28(4), pp. 258-281. doi.org/10.1080/01457630601117799

[22] Sivashanmugam. P., and Suresh, S., 2006, "Experimental studies on heat transfer and friction factor characteristics of laminar flow through a circular tube fitted with helical screw-tape inserts," Applied Thermal Engineering, 26, pp.1990-1997.

[23] Jaisankar, S., Radhakrishnan, T. K., and Sheeba, K. N., 2009, "Experimental studies on heat transfer and friction factor characteristics of thermosyphon solar water heater system fitted with spacer at the trailing edge of twisted tapes," Applied Thermal Engineering, 29(5-6), pp.1224-1231. doi.org/10.1016/j.applthermaleng.2008.06.009

[24] Rout, P.K., and Saha, S.K., 2013, "Laminar flow heat transfer and pressure drop in a circular tube having wire-coil and helical screw-tape inserts," Journal of Heat Transfer, 135(2), pp.021901. doi: 10.1115/1.4007415

[25] Saha, S. K., 2010, "Thermal and friction characteristics of laminar flow through rectangular and square ducts with transverse ribs and wire coil inserts," Experimental Thermal Fluid Science, 34(1), pp.63-72.

[26] Saha, S. K., 2013, "Thermohydraulics of laminar flow through a circular tube having integral helical corrugations and fitted with helical screw-tape insert," Chemical Engineering Communications, 200(3), pp. 418-436. doi.org/10.1080/00986445.2012.712579

[27] Pal, P. K., and Saha, S. K., 2010. "Thermal and friction characteristics of laminar flow through square and rectangular ducts with transverse ribs and twisted tapes with and without oblique teeth." Journal of Enhanced Heat Transfer, 17 (1).
DOI: 10.1615/JEnhHeatTransf.v17.i1.10

[28] Saha, S., 2011. "Thermohydraulics of turbulent flow through square and rectangular ducts with transverse ribs and twisted tapes with and without oblique teeth," Journal of Enhanced Heat Transfer, 18(4). DOI: 10.1615/JEnhHeatTransf.v18.i4.30

[29] Saha, S.K., Barman, B.K., and Banerjee, S., 2012. "Heat transfer enhancement of laminar flow through a circular tube having wire coil inserts and fitted with centre-cleared twisted tape," Journal of Thermal Science and Engineering Applications, 4(3), pp 031003. doi:10.1115/1.4006289

[30] Pramanik, D., and Saha, S.K., 2006. Thermohydraulics of laminar flow through rectangular and square ducts with transverse ribs and twisted tapes. Journal of Heat Transfer, 128(10), pp. 1070-1080. doi:10.1115/1.2345432

[31] Saha, S.K., and Langille, P., 2002. "Heat transfer and pressure drop characteristics of laminar flow through a circular tube with longitudinal strip inserts under uniform wall heat flux," Journal of Heat Transfer, 124(3), pp.421-432. DOI: 10.1115/1.1423907

[32] Saha, S., 2011. "Thermohydraulics of turbulent flow through square and rectangular ducts with transverse ribs and twisted tapes with and without oblique teeth," Journal of Enhanced Heat Transfer, 18(4). DOI: 10.1615/JEnhHeatTransf.v18.i4.30

[33] Oztop, H.F., 2005. "Effective parameters on second law analysis for semicircular ducts in laminar flow and constant wall heat flux," International Communications in Heat and Mass Transfer, 32(1-2), pp. 266-274

[34] Dagtekin, I., Oztop, H.F., Sahin, A. Z., 2005 "An analysis of entropy generation through a circular duct with different shaped longitudinal fins for laminar flow," International Journal of Heat and Mass Transfer, 48(1), pp. 171-181

[35] Kline, S. J., and McClintock, F. A., 1953, "Describing uncertainties in single sample experiments," Mechanical Engineering, 75(1), pp. 3-8.

[36] Saha, S., and Saha, S.K., 2013, "Enhancement of heat transfer of laminar flow through a circular tube having integral helical rib roughness and fitted with wavy strip inserts," Experimental Thermal and Fluid Science, 50, pp. 107-113.

doi.org/10.1016/j.expthermflusci.2013.05.010

[37] Saha, S. K., Bhattacharyya, S., and Dayanidhi, G. L., 2012, "Enhancement of heat transfer of laminar flow of viscous oil through a circular tube having integral axial rib roughness and fitted with helical screw-tape inserts," Heat Transfer Research, 43(2), pp. 1-21. doi/10.1615/HeatTransRes.2012004268

[38] Pal, P. K., and Saha, S. K., 2014, "Experimental investigation of laminar flow through a circular tube fitted with spiral corrugation and twisted tapes with oblique teeth," Experimental Thermal Fluid Science, 57, pp. 301-309.

doi.org/10.1016/j.expthermflusci.2014.05.007

[39] Tiwari, M., and Saha, S. K., 2015, "Laminar flow through a circular tube having transverse ribs and twisted tapes," International Journal of Advanced Technology in Engineering and Science, 3 (11), pp. 220-224. doi: 10.1115/1.4030792

[40] Bhattacharyya, S., Saha, S., and Saha, S. K., 2013, "Laminar flow heat transfer enhancement in a circular tube having integral transverse rib roughness and fitted with centre-cleared twisted-tape," Experimental Thermal Fluid Science, 44, pp. 727-735. doi.org/10.1016/j.expthermflusci.2012.09.016

[41] Bergles, A. E., Blumenkrantz, A. R., and Taborek, J., 1974, "Performance Evaluation Criteria for Enhanced Heat Transfer Surfaces," Paper FC 6.3, Proceedings of 5th International Heat Transfer Conference, Tokyo, 2, pp. 239-243.